International Journal of Solids and Structures 48 (2011) 2102–2119

Contents lists available at ScienceDirect

International Journal of Solids and Structures

journal homepage: www.elsevier.com/locate/ijsolstr

The effect of anisotropic damage evolution on the behavior of ductile and brittle matrix composites

Jacob Aboudi *

Faculty of Engineering, Tel-Aviv University, Ramat-Aviv 69978, Israel

ARTICLE INFO

Article history:
Received 30 August 2010
Received in revised form 1 February 2011
Available online 23 March 2011

Keywords:
Continuum damage mechanics
Damage evolution law
Anisotropic damage
Full thermomechanical coupling
High fidelity generalized method of cells

ABSTRACT

Anisotropic damage evolution laws for ductile and brittle materials have been coupled to a micromechanical model for the prediction of the behavior of composite materials. As a result, it is possible to investigate the effect of anisotropic progressive damage on the macroscopic (global) response and the local spatial field distributions of ductile and brittle matrix composites. Two types of thermoinelastic micromechanics analyses have been employed. In the first one, a one-way thermomechanical coupling in the constituents is considered according to which the thermal field affects the mechanical deformations. In the second one, a full thermomechanical coupling exists such that there is a mutual interaction between the mechanical and thermal fields via the energy equations of the constituents. Results are presented that illustrate the effect of anisotropic progressive damage in the ductile and brittle matrix phases on the composite's behavior by comparisons with the corresponding isotropic damage law and/or by tracking the components of the damage tensor.

1. Introduction

In the most general formulation of the continuum damage mechanics, the damage state should be represented by a fourth-order tensor. Such a formulation however would be too difficult and not necessary, Voyiadjis and Kattan (2005) and Lemaitre and Desmorat (2005). Theories with scalar damage variables are the easiest to handle. Anisotropic damage theories are based on second-order damage state representations. Discussions and presentations of continuum damage mechanics and the various formulations of the damage states and their evolution laws can be found in the books by Kachanov (1986), Lemaitre and Chaboche (1990), Krajcinovic (1996), Lemaitre (1996), Voyiadjis and Kattan (2005), and Lemaitre and Desmorat (2005), for example. Applications of continuum damage mechanics theories on composites materials are given by Talreja (1985a,b, 1994), Voyiadjis and Deliktas (1997) Voyiadjis and Kattan (1999), Skrzypek and Ganczarski (1999), Barbero (2008), Haj-Ali (2009), Bednarcyk et al. (2010), Haj-Ali and Aboudi (2010) and references cited there.

Lemaitre et al. (2000) presented a continuum damage theory with anisotropic damage evolution in ductile materials that generalizes the isotropic damage theory of Lemaitre (1985a,b) which is based on a scalar variable. In addition, Lemaitre and Desmorat (2005) presented anisotropic damage model for a brittle material (concrete). The purpose of the present investigation is to couple these theories with a micromechanics model for the prediction of the response of ductile and brittle matrix composites with evolving damage. As is shown in this investigation, the resulting micromechanics analyses enable the study of the effect of anisotropic damage laws by comparisons with the corresponding isotropic damage theories and by tracking the evolutions of the components of the damage tensor.

The micromechanics model that is employed in the present investigation is referred to as *The High Fidelity Generalized Method of Cells* (HFGMC) which is based on the homogenization procedure for periodic multiphase composites. This micromechanics model has been reviewed by Aboudi (2004) and more recently has been shown by Haj-Ali and Aboudi (2009) to provide excellent prediction for (undamaged) nonlinear and inelastic matrix composites by extensive comparisons with finite element solutions. In addition, this micromechanics model has been coupled by these authors to a finite element software to investigate the response of metal matrix composite structures.

This paper is organized as follows. In Section 2, the isotropic and anisotropic damage theories in unreinforced ductile materials are presented. This is follows by the presentation of the anisotropic damage theory of a brittle material. In Section 3, the HFGMC micromechanics theory is outlined. This includes the one-way and fully coupled thermoinelastic HFGMC. In the former theory, the conventional constitutive equations is employed according to which the thermal effects in the constituent affect the mechanical response of the material. In the latter theory, the fully coupled

* Tel.: +972 3 640 8131; fax: +972 3 640 7617.
E-mail address: aboudi@eng.tau.ac.il

0020-7683/$ - see front matter © 2011 Elsevier Ltd. All rights reserved.
doi:10.1016/j.ijsolstr.2011.03.014

HFGMC is discussed according to which, a mutual interaction exists between the mechanical and temperature fields in the constituents (Aboudi, 2008). This mutual interaction between the mechanical and thermal effects is governed by the coupled energy equation of the constituents. Due to the inelasticity effects in the metallic matrix, a major part of the rate of plastic work is liberated as a heat source to be included in the energy equation. The most interesting result from the fully coupled HFGMC theory are the spatial temperature distributions in the composite which are induced by the externally applied mechanical loadings. The generation of these temperature distributions enables the identification of critical hot spots in the composite caused by the mechanical loading. These hot spots indicate the existence of high inelastic strains which my lead to ultimate failure. In Section 4, extensive comparisons between the effects of anisotropic and isotropic damage laws in the ductile phase of metal matrix composites are presented. For the brittle matrix composite, the effect of anisotropic damage can be evaluated by tracking the evolution of the components of the damage tensor. Finally, a Conclusion section discusses possible future investigations.

2. Constitutive equations of the monolithic materials with progressive damage

2.1. Ductile materials with isotropic evolving damage

For thermoelastoplastic materials, the total strain tensor is decomposed, in the framework of the infinitesimal strain theory, into elastic, thermal and plastic components in the form:

$$\boldsymbol{\epsilon} = \boldsymbol{\epsilon}^e + \boldsymbol{\epsilon}^t + \boldsymbol{\epsilon}^p \tag{1}$$

The constitutive equations of these materials with isotropic damage law can be determined from the Gibbs potential G (per unit volume) as follows

$$\boldsymbol{\epsilon} = \frac{\partial G}{\partial \boldsymbol{\sigma}} = \frac{\partial G_{et}}{\partial \boldsymbol{\sigma}} + \boldsymbol{\epsilon}^p \tag{2}$$

where $\boldsymbol{\sigma}$ is the stress tensor and G_{et} is the thermoelastic portion of G. The expression for the thermoelastic contribution G_{et} is given by (Lemaitre and Desmorat, 2005):

$$G_{et} = \frac{1+\nu}{2E}\frac{\boldsymbol{\sigma}:\boldsymbol{\sigma}}{1-D} - \frac{\nu}{2E}\frac{tr^2(\boldsymbol{\sigma})}{1-D} + \alpha(T-T_0)tr(\boldsymbol{\sigma}) \tag{3}$$

where $tr(\boldsymbol{\sigma})$ is the trace of the stress tensor, $\boldsymbol{I}$ is the identity second-order tensor, $0 \leqslant D \leqslant 1$ is the damage variable, $T - T_0$ is the temperature deviation from a reference temperature T_0 and E, ν and α are the Young's modulus, Poisson's ratio and coefficient of thermal expansion of the isotropic material. Consequently, the following expression for the elastic and thermal strains is obtained

$$\boldsymbol{\epsilon}^e + \boldsymbol{\epsilon}^t = \frac{\partial G_{et}}{\partial \boldsymbol{\sigma}} = \frac{1+\nu}{E}\tilde{\boldsymbol{\sigma}} - \frac{\nu}{E}tr(\tilde{\boldsymbol{\sigma}})\boldsymbol{I} + \alpha(T-T_0)\boldsymbol{I} \tag{4}$$

with $\tilde{\boldsymbol{\sigma}}$ being the effective stress which is related to the stress $\boldsymbol{\sigma}$ in the form: $\tilde{\boldsymbol{\sigma}} = \boldsymbol{\sigma}/(1-D)$. This equation provides the following expression for the stress and effective stress tensors:

$$\boldsymbol{\sigma} = (1-D)\boldsymbol{h} : \boldsymbol{\epsilon}^e \tag{5}$$

and

$$\tilde{\boldsymbol{\sigma}} = \boldsymbol{h} : \boldsymbol{\epsilon}^e \tag{6}$$

with $\boldsymbol{h}$ being the standard forth-order stiffness tensor of isotropic materials

$$\boldsymbol{h} = \lambda \boldsymbol{I} \otimes \boldsymbol{I} + 2\mu \boldsymbol{I}_4 \tag{7}$$

where λ and μ are the Lame' constants and $\boldsymbol{I}_4$ is the forth-order unit tensor. It should be noted that Eq. (6) is based on the principle of strain equivalence according to which the strains in the damaged and effective configurations are equal. Hence, the strain constitutive equations of the damaged material are derived from the corresponding equations of the undamaged material by replacing stress in the latter by the equivalent stress.

By assuming isotropic hardening, the yield function ϕ is given by

$$\phi = \tilde{\sigma}_{eq} - \sigma_y = \frac{1}{1-D}\sigma_{eq} - \sigma_y \tag{8}$$

where X_{eq} of the second-order tensor $\boldsymbol{X}$ stands for

$$X_{eq} = \sqrt{\frac{3}{2}dev(\boldsymbol{X}) : dev(\boldsymbol{X})} = \sqrt{\frac{3}{2}}\|dev(\boldsymbol{X})\| \tag{9}$$

and $dev(\boldsymbol{X})$ is the deviator of $\boldsymbol{X}$. In Eq. (8), σ_y is the function that describes the hardening of the elastoplastic material. For isotropic hardening it is given by

$$\sigma_y = Y_0 + K(R) \tag{10}$$

where Y_0 is the yield stress in simple tension and $K(R)$ describes the isotropic hardening law. For linear hardening: $K(R) = H_0 R$. The rate of hardening is given by

$$\dot{R} = -\dot{\gamma}\frac{\partial \phi}{\partial K} = \dot{\gamma} \tag{11}$$

where γ is the consistency parameter. The evolution of the plastic strains is given by

$$\dot{\boldsymbol{\epsilon}}^p = \dot{\gamma}\frac{\partial \phi}{\partial \boldsymbol{\sigma}} = \frac{3\dot{\gamma}}{2(1-D)}\frac{dev(\tilde{\boldsymbol{\sigma}})}{\tilde{\sigma}_{eq}} = \sqrt{\frac{3}{2}}\frac{\dot{\gamma}}{1-D}\frac{dev(\boldsymbol{\sigma})}{\|dev(\boldsymbol{\sigma})\|} \tag{12}$$

The equivalent plastic strain can be obtained from this equation as follows

$$\dot{\epsilon}_p = \sqrt{\frac{2}{3}}\|\dot{\boldsymbol{\epsilon}}^p\| = \frac{\dot{\gamma}}{1-D} \tag{13}$$

The energy release rate Y is given in the form (Lemaitre and Desmorat, 2005)

$$\begin{aligned} Y &= -\frac{1}{2}\boldsymbol{\epsilon}^e : \boldsymbol{h} : \boldsymbol{\epsilon}^e = -\frac{\tilde{\sigma}_{eq}^2}{2E}\left[\frac{2}{3}(1+\nu) + 3(1-2\nu)\left(\frac{\sigma_H}{\sigma_{eq}}\right)^2\right] \\ &= -\frac{\sigma_{eq}^2}{2E(1-D)^2}\left[\frac{2}{3}(1+\nu) + 3(1-2\nu)\left(\frac{\sigma_H}{\sigma_{eq}}\right)^2\right] \end{aligned} \tag{14}$$

where $\sigma_H = tr(\boldsymbol{\sigma})/3$ being the hydrostatic stress.

Finally, the dissipation function ψ, also referred to as inelastic potential function, from which the inelastic flow rule and the evolution laws for the internal variables and damage are derived. It is taken in the form

$$\psi = \phi + \frac{S}{(1-D)(s+1)}\left(\frac{-Y}{S}\right)^{s+1} \tag{15}$$

where S and s are material constants. This function provides the isotropic evolution law of damage in the form

$$\dot{D} = -\dot{\gamma}\frac{\partial \psi}{\partial Y} = \frac{\dot{\gamma}}{1-D}\left(\frac{-Y}{S}\right)^s \tag{16}$$

The above system of nonlinear equations together with the condition that $\phi = 0$ that govern the behavior of monolithic thermoelastolplastic materials with isotropic evolving damage are solved incrementally in conjunction with the return mapping algorithm (de Souza Neto et al., 2008).

2.2. Ductile materials with anisotropic evolving damage

The formulation of the constitutive equations for elastoplastic materials with anisotropic damage law has been presented by Lemaitre et al. (2000). Presently, the damage is described by a second-order tensor $\boldsymbol{D}$ and the thermoelastic portion G_{et} is given by

$$G_{et} = \frac{1+\nu}{2E}\boldsymbol{H}dev(\boldsymbol{\sigma})\boldsymbol{H}dev(\boldsymbol{\sigma}) + \frac{3(1-2\nu)}{2E}\frac{\sigma_H^2}{1-\eta D_H} + \alpha(T-T_0)tr(\boldsymbol{\sigma}) \tag{17}$$

or in an equivalent indicial notation

$$G_{et} = \frac{1+\nu}{2E}H_{ij}\hat{\sigma}_{jk}H_{kl}\hat{\sigma}_{li} + \frac{3(1-2\nu)}{2E}\frac{\sigma_H^2}{1-\eta D_H} + \alpha(T-T_0)\sigma_{kk}$$

where $\hat{\sigma}_{ij}$ is the deviator of σ_{ij}, and

$$\mathbf{H} = (\mathbf{I}-\mathbf{D})^{-1/2} \tag{18}$$

$D_H = tr(\boldsymbol{D})/3$ and η is a material parameter.

The elastic strain is obtained from Eq. (17) as

$$\boldsymbol{\epsilon}^e = \frac{1+\nu}{E}\tilde{\boldsymbol{\sigma}} - \frac{\nu}{E}tr(\tilde{\boldsymbol{\sigma}})\boldsymbol{I} \tag{19}$$

The relation between the effective stress $\tilde{\boldsymbol{\sigma}}$ and the stress $\boldsymbol{\sigma}$ is given by

$$\tilde{\boldsymbol{\sigma}} = dev[\boldsymbol{H}dev(\boldsymbol{\sigma})\boldsymbol{H}] + \frac{\sigma_H}{1-\eta D_H}\boldsymbol{I} \tag{20}$$

The effective stress $\tilde{\boldsymbol{\sigma}}$ is related to the elastic strain $\boldsymbol{\epsilon}^e$ as is given by Eq. (6).

The yield function is given by

$$\phi = \tilde{\sigma}_{eq} - \sigma_y \tag{21}$$

The evolution law for the plastic strains is

$$\dot{\boldsymbol{\epsilon}}^p = \dot{\gamma}\frac{\partial\phi}{\partial\boldsymbol{\sigma}} = \frac{3}{2}\dot{\gamma}\frac{dev[\boldsymbol{H}dev(\tilde{\boldsymbol{\sigma}})\boldsymbol{H}]}{\tilde{\sigma}_{eq}} \tag{22}$$

The rate of the equivalent plastic strain is accordingly given by

$$\dot{\epsilon}_p = \dot{\gamma}\frac{[\boldsymbol{H}dev(\tilde{\boldsymbol{\sigma}})\boldsymbol{H}]_{eq}}{\tilde{\sigma}_{eq}} \tag{23}$$

The evolution law for the damage tensor $\boldsymbol{D}$ is given according to Lemaitre et al. (2000) by

$$\dot{\boldsymbol{D}} = \left(\frac{-Y}{S}\right)^s |\dot{\boldsymbol{\epsilon}}^p| \tag{24}$$

where $|\dot{\boldsymbol{\epsilon}}^p|$ means the absolute value of the eigenvalues of tensor $\dot{\boldsymbol{\epsilon}}^p$. In this equation, the damage energy release rate Y is given by

$$Y = -\frac{1}{2}\boldsymbol{\epsilon}^e : \boldsymbol{h} : \boldsymbol{\epsilon}^e = -\frac{\tilde{\sigma}_{eq}^2}{2E}\left[\frac{2}{3}(1+\nu) + 3(1-2\nu)\left(\frac{\tilde{\sigma}_H}{\tilde{\sigma}_{eq}}\right)^2\right] \tag{25}$$

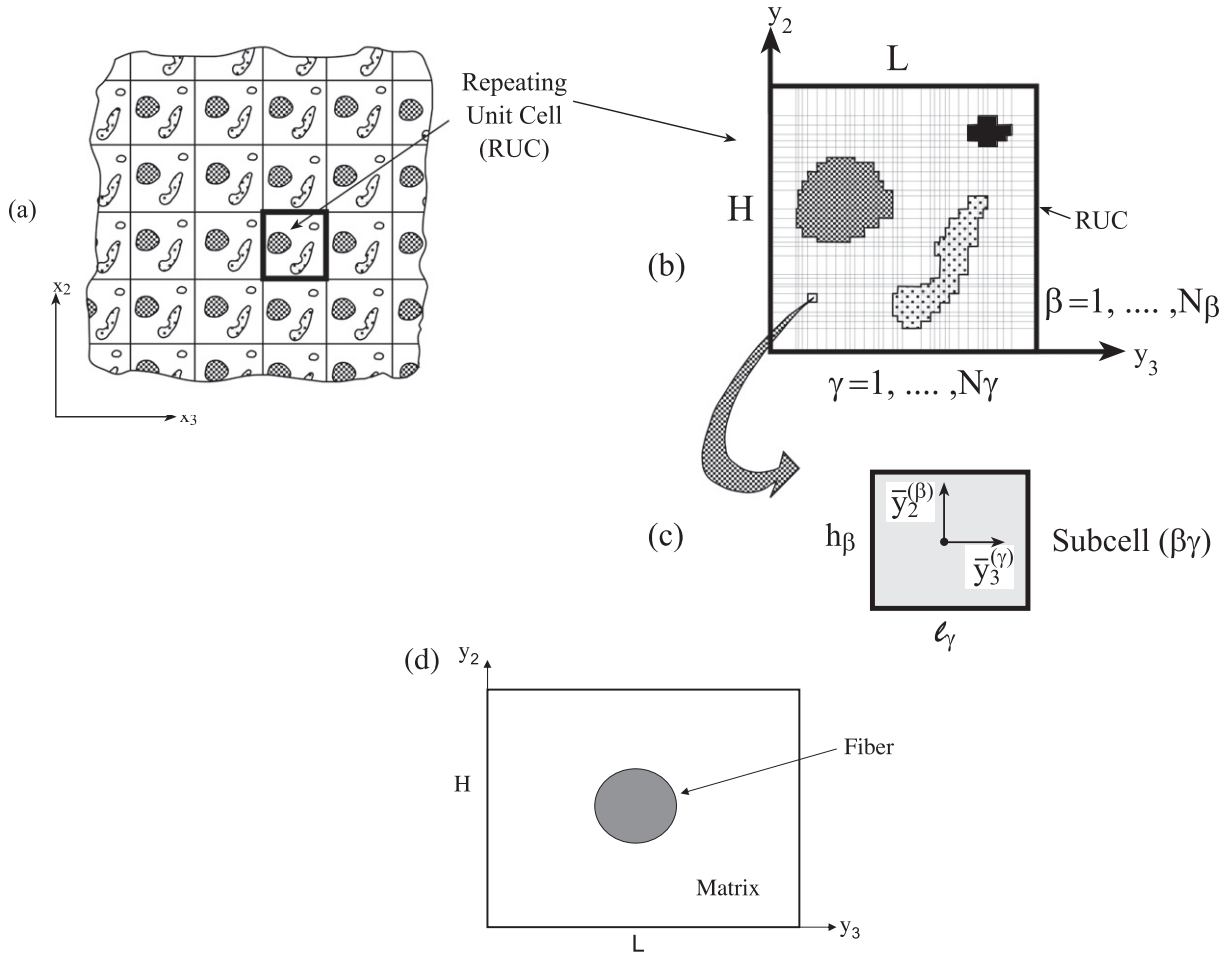

Fig. 1. (a) A multiphase composite with doubly-periodic microstructures defined with respect to global coordinates (x_2,x_3). (b) The repeating unit cell is represented with respect to local coordinates (y_2,y_3). It is divided into N_β and N_γ subcells, in the y_2 and y_3 directions, respectively. (c) A characteristic subcell ($\beta\gamma$) with local coordinates $\bar{y}_2^{(\beta)}$ and $\bar{y}_3^{(\gamma)}$ whose origin is located at its center. (d) A typical repeating unit cell with a fiber oriented in the 1-direction reinforcing a ductile or brittle matrix.

where

$$\tilde{\sigma}_H = \frac{\sigma_H}{1-\eta D_{kk}/3}$$

In order to implement the present theory, the explicit relation between the stress $\boldsymbol{\sigma}$ and the effective stress $\tilde{\boldsymbol{\sigma}}$ must be established. From Eq. (20), the following expression can be readily established in the principal coordinates in which $\boldsymbol{D} = diag(D_1,D_2,D_3)$ so that $\boldsymbol{H} = diag\left(1/\sqrt{1-D_1}, 1/\sqrt{1-D_2}, 1/\sqrt{1-D_3}\right)$:

$$\begin{Bmatrix} \tilde{\sigma}_{11} \\ \tilde{\sigma}_{22} \\ \tilde{\sigma}_{33} \\ \tilde{\sigma}_{23} \\ \tilde{\sigma}_{13} \\ \tilde{\sigma}_{12} \end{Bmatrix} = \begin{bmatrix} K_{11} & K_{12} & K_{13} & 0 & 0 & 0 \\ & K_{22} & K_{23} & 0 & 0 & 0 \\ & & K_{33} & 0 & 0 & 0 \\ & & & K_{44} & 0 & 0 \\ & & & & K_{55} & 0 \\ \text{sym.} & & & & & K_{66} \end{bmatrix} \begin{Bmatrix} \sigma_{11} \\ \sigma_{22} \\ \sigma_{33} \\ \sigma_{23} \\ \sigma_{13} \\ \sigma_{12} \end{Bmatrix} \tag{26}$$

where

$$K_{11} = \frac{4}{9(1-D_1)} + \frac{1}{9(1-D_2)} + \frac{1}{9(1-D_3)} + \frac{1}{3(1-\eta D_H)}$$

$$K_{12} = -\frac{2}{9(1-D_1)} - \frac{2}{9(1-D_2)} + \frac{1}{9(1-D_3)} + \frac{1}{3(1-\eta D_H)}$$

$$K_{13} = -\frac{2}{9(1-D_1)} + \frac{1}{9(1-D_2)} - \frac{2}{9(1-D_3)} + \frac{1}{3(1-\eta D_H)}$$

$$K_{22} = \frac{1}{9(1-D_1)} + \frac{4}{9(1-D_2)} + \frac{1}{9(1-D_3)} + \frac{1}{3(1-\eta D_H)}$$

$$K_{23} = \frac{1}{9(1-D_1)} - \frac{2}{9(1-D_2)} - \frac{2}{9(1-D_3)} + \frac{1}{3(1-\eta D_H)}$$

$$K_{33} = \frac{1}{9(1-D_1)} + \frac{1}{9(1-D_2)} + \frac{4}{9(1-D_3)} + \frac{1}{3(1-\eta D_H)}$$

$$K_{44} = \frac{1}{\sqrt{(1-D_2)(1-D_3)}}$$

$$K_{55} = \frac{1}{\sqrt{(1-D_1)(1-D_3)}}$$

$$K_{66} = \frac{1}{\sqrt{(1-D_1)(1-D_2)}}$$

It should be noted that in the absence of damage $\boldsymbol{K}$ reduces to the unit matrix.

The above relation can be inverted in order to express $\boldsymbol{\sigma}$ in terms of $\tilde{\boldsymbol{\sigma}}$:

$$\boldsymbol{\sigma} = \boldsymbol{L}\tilde{\boldsymbol{\sigma}} \tag{27}$$

where $\boldsymbol{L} = \boldsymbol{K}^{-1}$. Consequently, by employing Eq. (6) the following constitutive relation can be established

$$\begin{Bmatrix} \sigma_{11} \\ \sigma_{22} \\ \sigma_{33} \\ \sigma_{23} \\ \sigma_{13} \\ \sigma_{12} \end{Bmatrix} = \begin{bmatrix} L_{11} & L_{12} & L_{13} & 0 & 0 & 0 \\ & L_{22} & L_{23} & 0 & 0 & 0 \\ & & L_{33} & 0 & 0 & 0 \\ & & & L_{44} & 0 & 0 \\ & & & & L_{55} & 0 \\ \text{sym.} & & & & & L_{66} \end{bmatrix} \times \begin{bmatrix} \lambda+2\mu & \lambda & \lambda & 0 & 0 & 0 \\ & \lambda+2\mu & \lambda & 0 & 0 & 0 \\ & & \lambda+2\mu & 0 & 0 & 0 \\ & & & \mu & 0 & 0 \\ & & & & \mu & 0 \\ \text{sym.} & & & & & \mu \end{bmatrix} \begin{Bmatrix} \epsilon^e_{11} \\ \epsilon^e_{22} \\ \epsilon^e_{33} \\ 2\epsilon^e_{23} \\ 2\epsilon^e_{13} \\ 2\epsilon^e_{12} \end{Bmatrix} \tag{28}$$

Relation (28) provides at any instant of loading the current stiffness matrix $\boldsymbol{C} = \boldsymbol{LM}$ ($\boldsymbol{M}$ denotes the standard second matrix in the above relation). In the isotropic damage law, on the other hand, the current stiffness matrix was simply given by $\boldsymbol{C} = (1-D)\boldsymbol{M}$. In the absence of damage Eq. (28) reduces to the Hooke's law of isotropic elastic materials.

The resulting system that governs the evolution of plasticity and anisotropic damage consists of ten nonlinear equations which are given by the six Eq. (6) in conjunction with relation (1), the three evolution Eq. (24) and the conditions that $\phi = 0$. The ten unknowns are $\tilde{\boldsymbol{\sigma}}, \Delta\gamma$ and the three principal damage variables. This system is solved in conjunction with the return mapping algorithm.

2.3. Brittle materials with anisotropic evolving damage

In brittle materials such as glass and ceramics, failure is characterized by the fact that damage evolution is the only dissipative mechanism that takes place, without irreversible strains. Although concrete is not a brittle material (see Wu et al. (2006) for example, where isotropic damage and inelasticity effects that develop in concrete are modeled), constitutive equations with anisotropic damage for concrete in which the plasticity effects are assumed to be negligible, have been proposed Lemaitre and Desmorat (2005). They are based on the following specific Gibbs function

Table 1
Elastic and thermal parameters of the transversely isotropic carbon fibers.

E_A (GPa)	E_T (GPa)	G_A (GPa)	v_A	v_T	α_A (10^{-6}/°C)	α_T (10^{-6}/°C)
388.2	7.6	14.9	0.41	0.45	−0.68	9.74

E_A, E_T, G_A, v_A, v_T, α_A and α_T denote the axial Young's modulus, transverse Young's modulus, axial shear modulus, axial Poisson's ratio, transverse Poisson's ratio, axial and transverse coefficients of thermal expansion, respectively.

Table 2
Material constants of the 2024 – *T*4 aluminum alloy (Aboudi, 1991).

Temperature (°C)	E (GPa)	v	α (10^{-6}/°C)	Y_0 (MPa)	H_0 (GPa)
21	72.4	0.33	22.5	286.7	11.7
148.9	69.3	0.33	22.5	270	10
204.4	65.7	0.33	22.5	225	8
260	58.4	0.33	22.5	140	3
371.1	41.5	0.33	22.5	42	0.4

E, v, α, Y_0 and H_0 denote the Young's modulus, Poisson's ratio, coefficient of thermal expansion, initial yield stress and linear hardening coefficient, respectively.

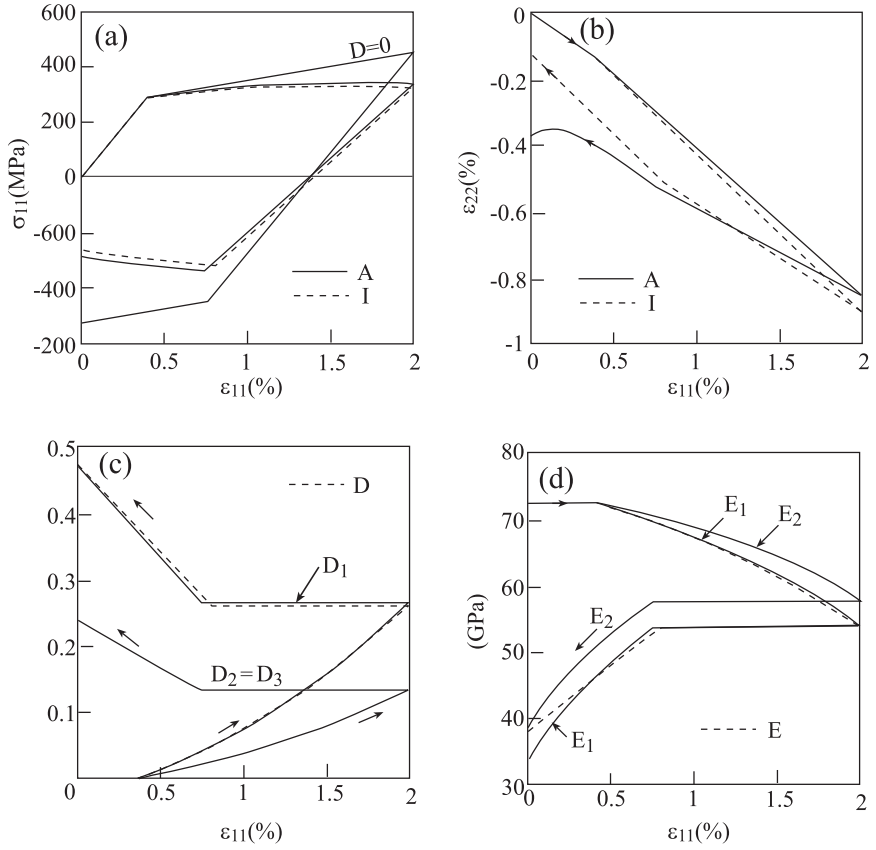

Fig. 2. The behavior of the aluminum alloy matrix subjected to a uniaxial stress loading–unloading with anisotropic (A) and isotropic (I) damage laws at room temperature. (a) Stress–strain response, (b) transverse-axial strain response, (c) evolution of the damage variables controlled by anisotropic and isotropic laws, (d) variation of the axial E_1 and transverse E_2 Young's moduli in the anisotropic case and of the Young's modulus E in the isotropic case.

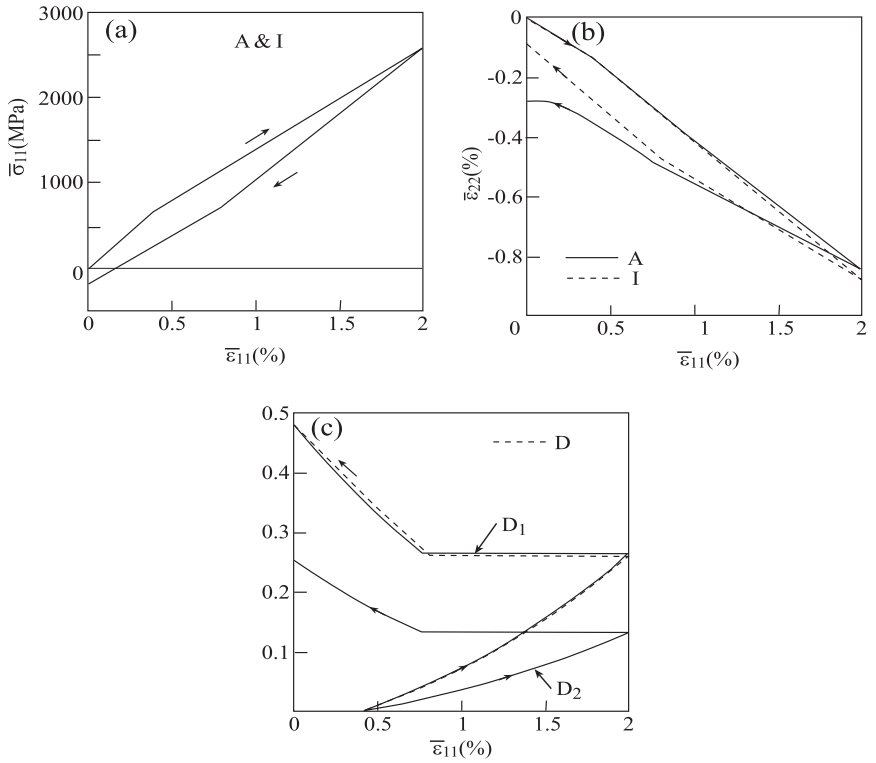

Fig. 3. The behavior of the unidirectional carbon/aluminum composite which is subjected to a uniaxial stress loading–unloading in the fibers direction at room temperature predicted by the anisotropic (A) and isotropic (I) evolution laws. (a) Global stress–strain response, (b) global transverse-axial strain response, (c) evolution of the matrix damage variables D_1, D_2 and D controlled by anisotropic and isotropic laws, respectively.

$$G = \frac{1+v}{2E} tr[\boldsymbol{H} dev(\boldsymbol{\sigma}) \boldsymbol{H} dev(\boldsymbol{\sigma})] + \frac{1-2v}{6E}\left[\frac{\langle tr(\boldsymbol{\sigma})\rangle^2}{1-tr(\boldsymbol{D})} + \langle -tr(\boldsymbol{\sigma})\rangle^2\right] \tag{29}$$

where $\langle x\rangle = x\,U(x)$, with $U(x)$ being the Heaviside unit step function and $\boldsymbol{H}$ is given by Eq. (18). From Eq. (29), the following expression for the strain tensor $\boldsymbol{\epsilon}$ in terms of the effective stress $\tilde{\boldsymbol{\sigma}}$ is obtained

$$\boldsymbol{\epsilon} = \frac{\partial G}{\partial \boldsymbol{\sigma}} = \frac{1+v}{E}\tilde{\boldsymbol{\sigma}} - \frac{v}{E} tr(\tilde{\boldsymbol{\sigma}})\boldsymbol{I} \tag{30}$$

where the effective stress tensor $\tilde{\boldsymbol{\sigma}}$ is given in terms of the stress $\boldsymbol{\sigma}$ as follows

$$\tilde{\boldsymbol{\sigma}} = dev[\boldsymbol{H} dev(\boldsymbol{\sigma})\boldsymbol{H}] + \frac{1}{3}\left[\frac{\langle tr(\boldsymbol{\sigma})\rangle}{1-tr(\boldsymbol{D})} - \langle -tr(\boldsymbol{\sigma})\rangle\right]\boldsymbol{I} \tag{31}$$

The initiation of damage in the present case is determined by the following condition

$$f(\boldsymbol{\epsilon}) = \epsilon^* - \kappa(tr(\boldsymbol{D})) > 0 \tag{32}$$

where the damage equivalent strain ϵ^* is defined in terms of the principal values ϵ_A, $A = 1, 2, 3$, of the strain tensor in the form

$$\epsilon^* = \sqrt{\langle\epsilon_1\rangle^2 + \langle\epsilon_2\rangle^2 + \langle\epsilon_3\rangle^2} \tag{33}$$

and the function $\kappa(tr\boldsymbol{D})$ is given by

$$\kappa(tr\boldsymbol{D}) = a\tan\left[\frac{tr\boldsymbol{D}}{aa^*} + \arctan\left(\frac{\kappa_0}{a}\right)\right] \tag{34}$$

where a', a are material constants and κ_0 is the damage threshold.

The damage evolution is controlled by

$$\dot{D}_A = a'\left[1 + \left(\frac{\epsilon^*}{a}\right)^2\right]^{-1} \frac{\dot{\epsilon}^*}{\epsilon^{*2}}\langle\epsilon_A\rangle^2, \quad A = 1,2,3 \tag{35}$$

Expansion of Eq. (31) yields the following relation expressed in terms of the principal values $\tilde{\sigma}_1$, $\tilde{\sigma}_2$, $\tilde{\sigma}_3$ of the effective stress and the principal values σ_1, σ_2, σ_3 of the stress tensors

$$\begin{Bmatrix}\tilde{\sigma}_1\\ \tilde{\sigma}_2\\ \tilde{\sigma}_3\end{Bmatrix} = \begin{bmatrix}K_{11} & K_{12} & K_{13}\\ & K_{22} & K_{23}\\ \text{sym.} & & K_{33}\end{bmatrix}\begin{Bmatrix}\sigma_1\\ \sigma_2\\ \sigma_3\end{Bmatrix} \tag{36}$$

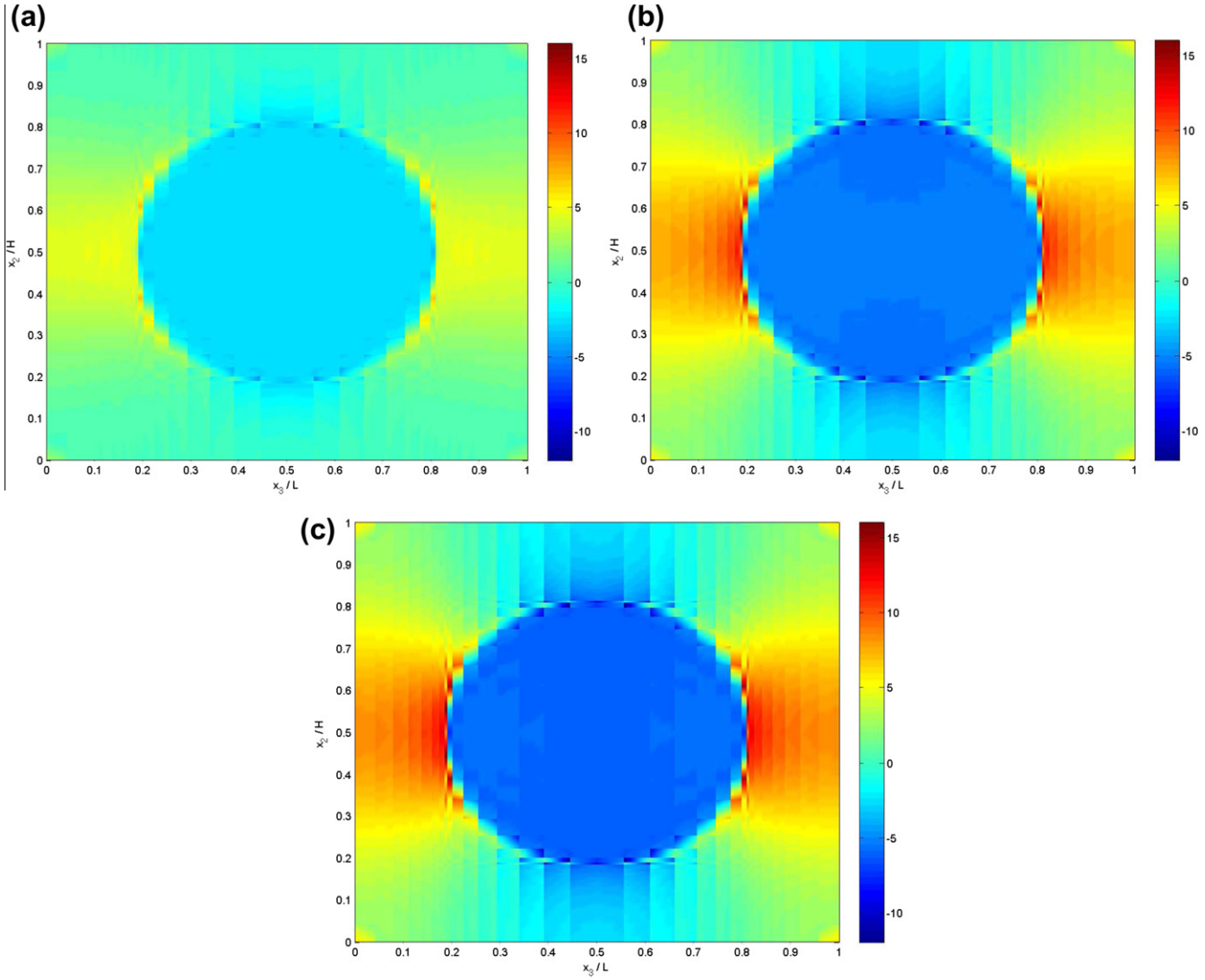

Fig. 4. Surface plots of the internal spatial transverse stress distributions σ_{22} in the RUC, generated by applying a longitudinal uniaxial stress loading of the carbon/aluminum composite at $\bar{\epsilon}_{11} = 0.02$ at room temperature. (a) σ_{22} distribution generated by the anisotropic damage law, (b) σ_{22} distribution generated by the isotropic damage law, (c) σ_{22} distribution generated in the absence of damage.

where

$$K_{11}=\frac{4}{9(1-D_1)}+\frac{1}{9(1-D_2)}+\frac{1}{9(1-D_3)}+\frac{U(\sigma_H)}{3(1-3D_H)}+\frac{1-U(\sigma_H)}{3}$$

$$K_{12}=-\frac{2}{9(1-D_1)}-\frac{2}{9(1-D_2)}+\frac{1}{9(1-D_3)}+\frac{U(\sigma_H)}{3(1-3D_H)}+\frac{1-U(\sigma_H)}{3}$$

$$K_{13}=-\frac{2}{9(1-D_1)}+\frac{1}{9(1-D_2)}-\frac{2}{9(1-D_3)}+\frac{U(\sigma_H)}{3(1-3D_H)}+\frac{1-U(\sigma_H)}{3}$$

$$K_{22}=\frac{1}{9(1-D_1)}+\frac{4}{9(1-D_2)}+\frac{1}{9(1-D_3)}+\frac{U(\sigma_H)}{3(1-3D_H)}+\frac{1-U(\sigma_H)}{3}$$

$$K_{23}=\frac{1}{9(1-D_1)}-\frac{2}{9(1-D_2)}-\frac{2}{9(1-D_3)}+\frac{U(\sigma_H)}{3(1-3D_H)}+\frac{1-U(\sigma_H)}{3}$$

$$K_{33}=\frac{1}{9(1-D_1)}+\frac{1}{9(1-D_2)}+\frac{4}{9(1-D_3)}+\frac{U(\sigma_H)}{3(1-3D_H)}+\frac{1-U(\sigma_H)}{3}$$

In the absence of damage, the matrix $\boldsymbol{K}$ reduces to the identity matrix. In conjunction with Eq. (30), the following principal stress–strain relations can be established

$$\begin{Bmatrix}\sigma_1\\ \sigma_2\\ \sigma_3\end{Bmatrix}=\begin{bmatrix}L_{11} & L_{12} & L_{13}\\ & L_{22} & L_{23}\\ \text{sym.} & & L_{33}\end{bmatrix}\begin{bmatrix}\lambda+2\mu & \lambda & \lambda\\ & \lambda+2\mu & \lambda\\ \text{sym.} & & \lambda+2\mu\end{bmatrix}\begin{Bmatrix}\epsilon_1\\ \epsilon_2\\ \epsilon_3\end{Bmatrix} \tag{37}$$

where the matrix $\boldsymbol{L}$ is the inverse of matrix $\boldsymbol{K}$. In the absence of damage, this equation reduces to the standard Hooke's law. For given values of the current applied strains, Eq. (37) forms a system of three nonlinear equations in the three unknown principal stresses. The current value if the stiffness matrix of the material is given by $\boldsymbol{C}=\boldsymbol{LM}$, where $\boldsymbol{M}$ is the second matrix in this equation. This matrix represents the current value of the principal stress derivatives

$$\boldsymbol{C}=\frac{d\boldsymbol{\sigma}}{d\boldsymbol{\epsilon}} \tag{38}$$

which is a function of the principal stresses. The full tensor derivative $d\boldsymbol{\sigma}/d\boldsymbol{\epsilon}$ (whose eigenvalues are given by Eq. (38)) can be obtained by employing the function derivative procedure that is described in de Souza Neto et al. (2008).

3. Micromechanical analysis

The HFGMC micromechanics model has been adopted to predict the behavior of metal matrix and concrete matrix unidirectionally reinforced composites. It is based, in conjunction with an averaging procedure, on the homogenization technique for composites with periodic microstructure as shown in Fig. 1(a) in terms of the global coordinates (x_1,x_2,x_3) with x_1 being the direction of the fibers. The rectangular repeating unit cell (RUC), Fig. 1(b), is defined with respect to the local coordinates (y_1,y_2,y_3) and is divided into N_β and N_γ subcells in the y_2 and y_3 directions respectively. Each subcell is labeled by the indices $(\beta\gamma)$ with $\beta=1,\ldots,N_\beta$, $\gamma=1,\ldots,N_\gamma$ and may contain a distinct homogeneous material. A brief outline of the HFGMC model is given in a compact form in the following but for details see Aboudi (2004).

The constitutive equations of the material in subcell $(\beta\gamma)$ can be represented in a general form as

$$\boldsymbol{\sigma}^{(\beta\gamma)}=\boldsymbol{C}^{(\beta\gamma)}:\left[\boldsymbol{\epsilon}^{(\beta\gamma)}-\boldsymbol{\epsilon}^{p(\beta\gamma)}-\boldsymbol{\epsilon}^{t(\beta\gamma)}\right] \tag{39}$$

where $\boldsymbol{C}^{(\beta\gamma)}$ is its current forth-order stiffness tensor. Two types of HFGMC micromechanics analysis are considered. In the first one, referred to as one-way thermomechanically coupled, a constant temperature that affects the mechanical field only is prescribed at any point of the composite's constituents. In the full thermomechanical coupling on the other hand, a mutual interaction exists between the mechanical and temperature fields. The latter is governed by the coupled energy equation in the subcell which includes in addition to the heat released by the plastic deformations, the power dissipated by the internal decohesion process. It is given by Lemaitre and Desmorat (2005)

$$\begin{aligned}\left(\rho c_v\right)^{(\beta\gamma)}\dot{T}^{(\beta\gamma)}+\nabla\cdot\boldsymbol{q}^{(\beta\gamma)}&=\boldsymbol{\sigma}^{(\beta\gamma)}:\dot{\boldsymbol{\epsilon}}^{p(\beta\gamma)}\\&\quad-T^{(\beta\gamma)}\boldsymbol{\Gamma}^{(\beta\gamma)}:\left[\dot{\boldsymbol{\epsilon}}^{(\beta\gamma)}-\dot{\boldsymbol{\epsilon}}^{p(\beta\gamma)}\right]-Y^{(\beta\gamma)}\dot{D}^{(\beta\gamma)}\end{aligned} \tag{40}$$

where $\rho^{(\beta\gamma)}, c_v^{(\beta\gamma)}$ and $\boldsymbol{q}^{(\beta\gamma)}$ denote the mass density, the specific heat at constant deformation and heat flux vector of the material filling subcell $(\beta\gamma)$, respectively. In addition, $\boldsymbol{\Gamma}^{(\beta\gamma)}$ is the thermal stress second-order tensor namely, the multiplication of the stiffness tensor $\boldsymbol{C}^{(\beta\gamma)}$ by the coefficient of the thermal expansion tensor $\boldsymbol{\alpha}$, i.e., $\boldsymbol{\Gamma}^{(\beta\gamma)}=\boldsymbol{C}^{(\beta\gamma)}:\boldsymbol{\alpha}^{(\beta\gamma)}$. The heat flux vector $\boldsymbol{q}^{(\beta\gamma)}$ is given by the Fourier's law

$$\boldsymbol{q}^{(\beta\gamma)}=-\boldsymbol{k}^{(\beta\gamma)}\cdot\nabla T^{(\beta\gamma)} \tag{41}$$

where $\boldsymbol{k}^{(\beta\gamma)}$ is the second-order thermal conductivity tensor. The effect of isotropic and anisotropic evolving damage on the

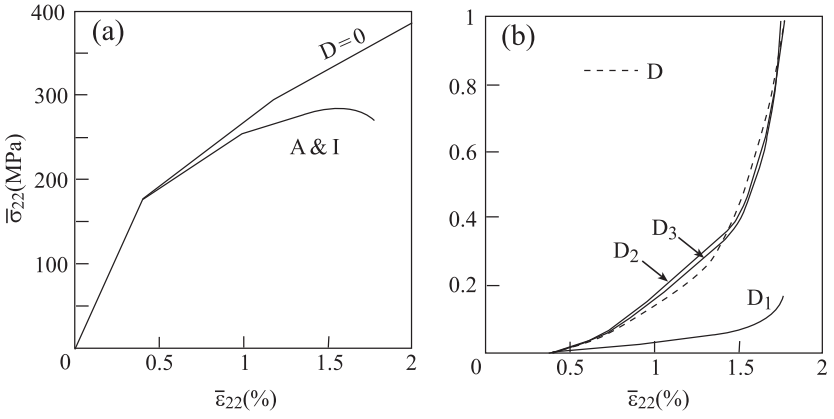

Fig. 5. The behavior of the unidirectional carbon/aluminum composite which is subjected to a transverse uniaxial stress loading at room temperature predicted by the anisotropic (A) and isotropic (I) evolution laws. (a) Global stress–strain response ($D=0$ corresponds to the response in the absence of damage), (b) evolution of the matrix damage variables D_1, D_2, D_3 and D controlled by anisotropic and isotropic laws, respectively.

composite's response can be investigated by employing these two micromechanics analyses. Both the one-way and fully thermomechanically coupled HFGMC have been discussed by Aboudi (2008). Herein a brief outline of the two HFGMC methods are presented.

3.1. HFGMC with one-way thermomechanical coupling

1. A quadratic displacement field is assumed in each subcell in terms of the local coordinates $(\bar{y}_2, \bar{y}_3)$, Fig. 1(c), with the expansions coefficients being the unknown microvariables.
2. The strong form of the equilibrium equations, tractions and displacements interfacial continuity conditions between the subcells and tractions and displacements periodic conditions between repeating unit cells are imposed in the average (integral) sense.
3. This results in a system of linear algebraic equations which is solved for the 15 unknown microvariable coefficients per subcell in terms of the constituents properties, microstructural dimensions and thermal and inelastic terms. (A statical condensation can reduce the number of unknowns to 6 per subcell, Haj-Ali and Aboudi, 2009).
4. Knowledge of the these microvariables enables the establishment of a localization relation that involves mechanical, thermal and inelastic concentration tensors. This localization relation relates the average strain in each subcell to the externally applied strains along with thermal and inelastic tensors.
5. The established mechanical, thermal and inelastic concentration tensors enable the establishment of the macroscopic (global) constitutive law of the composite with progressive damage in its phases at any instant of thermomechanical loading including, in particular, its current effective moduli.

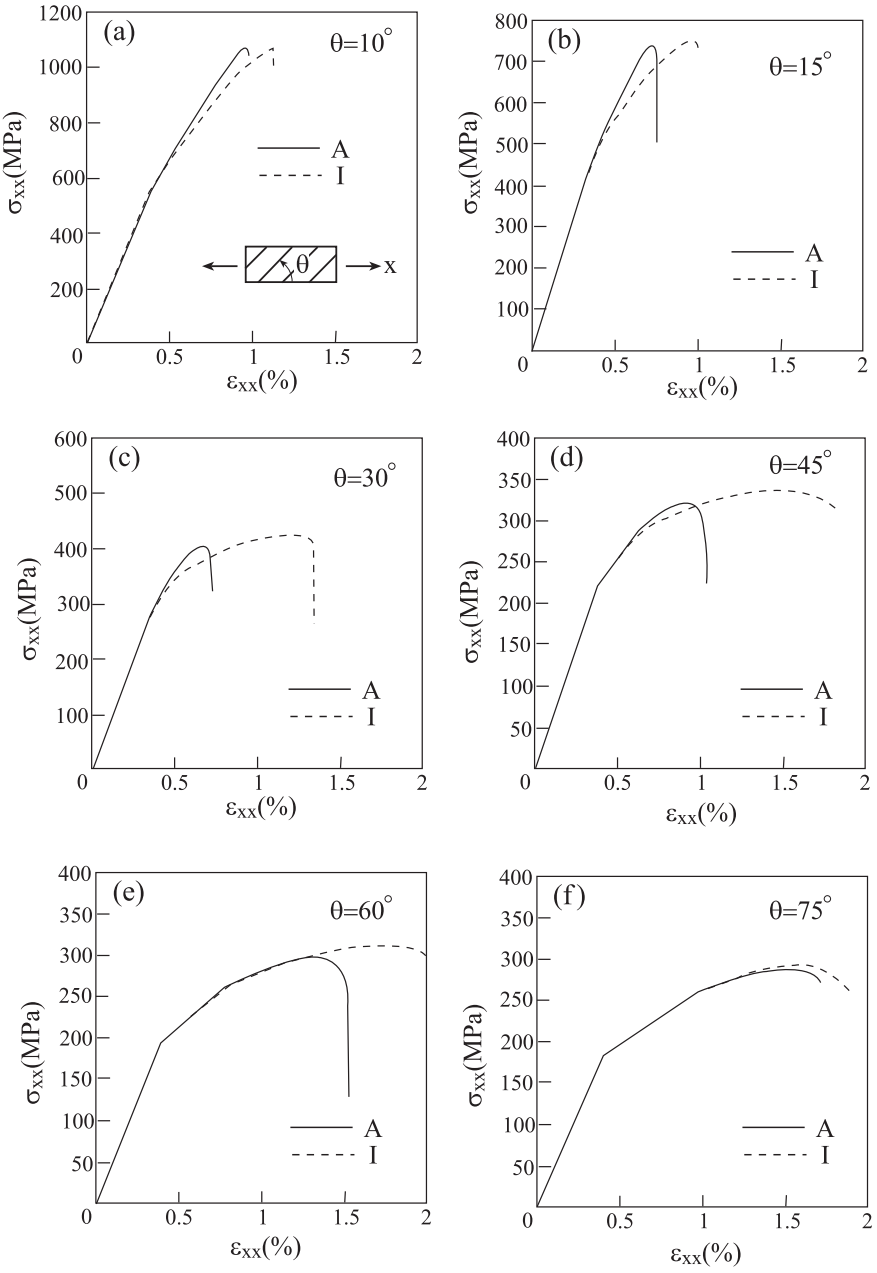

Fig. 6. The global stress-stress responses of the unidirectional carbon/aluminum composite that is subjected to off-axis uniaxial stress loading at various angles θ with respect to the fibers direction at room temperature. Comparison between the response predicted by the anisotropic (A) and isotropic (I) damage laws.

3.2. HFGMC with full thermomechanical coupling

1. A quadratic displacement and temperature fields are assumed in each subcell in terms of the local coordinates $(\bar{y}_2, \bar{y}_3)$, Fig. 1(c), with the expansions coefficients being the unknown displacement and thermal microvariables.
2. The strong form of the equilibrium and energy equations, tractions, displacements, heat fluxes and temperatures interfacial continuity conditions between the subcells, and tractions and displacements heat fluxes and temperatures periodic conditions between repeating unit cells are imposed in the average (integral) sense.
3. This results in a system of linear algebraic equations which is solved for the 22 unknown microvariable coefficients per subcell in terms of the constituents properties, microstructural dimensions and thermal and inelastic terms.

Items 4 and 5 are identical to the above. It should be emphasized however the application of the far-field strain induces this time a temperature deviation from the reference temperature due to the full thermomechanical coupling. These induced temperature deviations are significant in the presence of inelasticity effects in the constituents.

3.3. Micromechanical prediction of the composite's initial damage surfaces

Initial damage surfaces of metal matrix composites are identical to the initial yield surfaces. The method of their prediction have

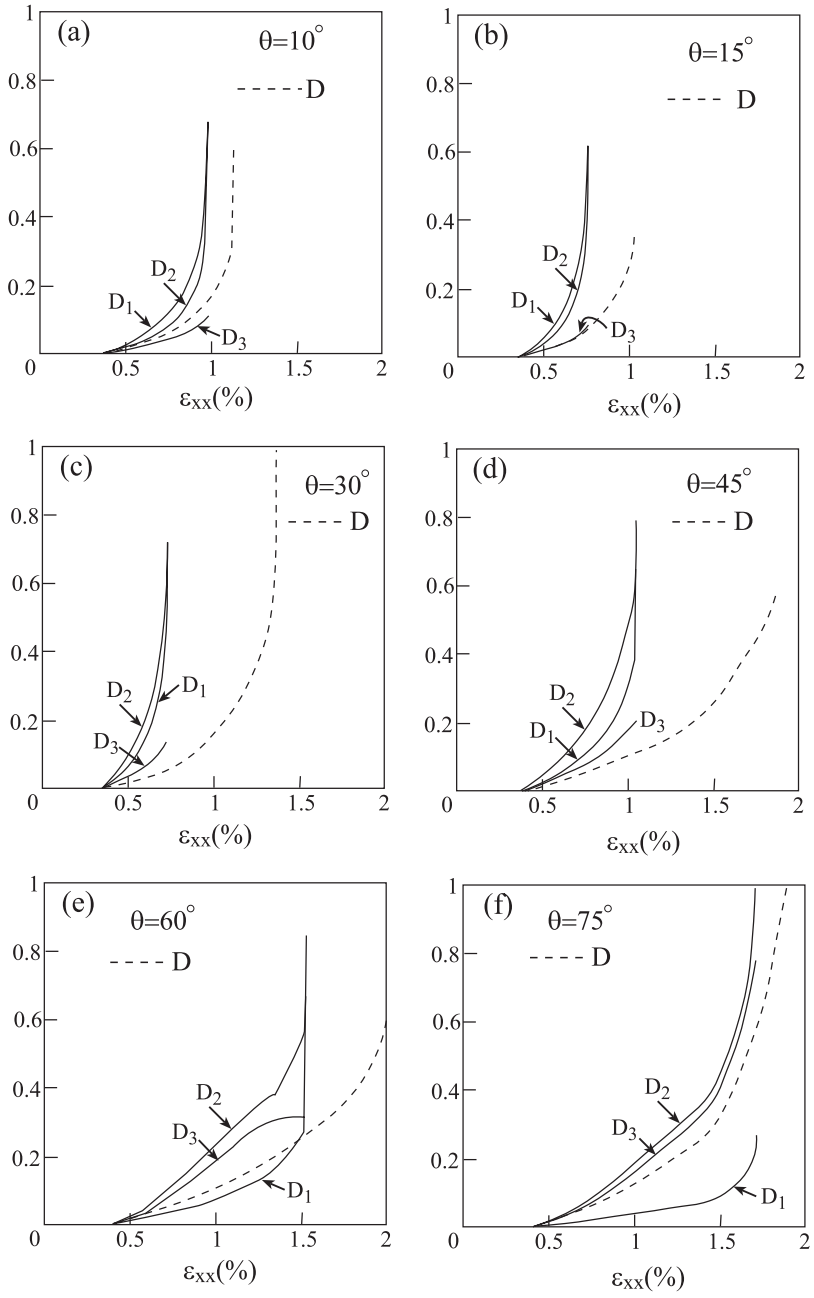

Fig. 7. The evolution of the damage variables D_1, D_2, D_3 and D obtained from the anisotropic and isotropic laws, respectively, in the metallic matrix caused by the off-axis loading of the unidirectional carbon/aluminum composite.

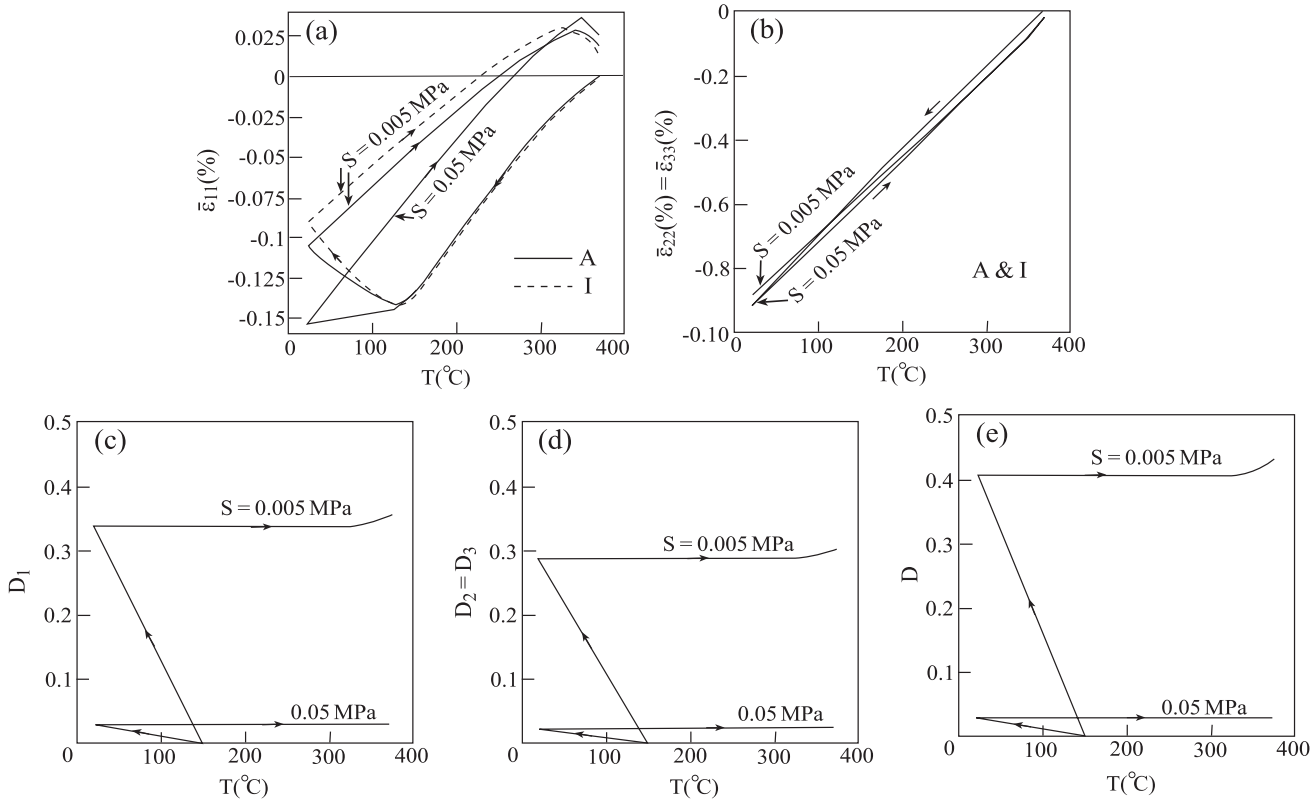

Fig. 8. The unidirectional carbon/aluminum composite is subjected to a temperature cycle of cooling and re-heating. (a) The developed macroscopic axial strain in the anisotropic and isotropic (I) cases, (b) the developed macroscopic transverse strain, (c)–(e) anisotropic damage variables D_1, $D_2 = D_3$ evolution, (f) isotropic damage variable D evolution.

Table 3
The material parameters of the concrete (Lemaitre and Desmorat, 2005).

E (GPa)	v	a'	a	κ_0
42	0.2	5000	2.93×10^{-4}	5×10^{-5}

E and v are the Young's modulus, Poisson's ratio, and a', a and κ_0 are nondimensional parameters.

been extensively discussed in Aboudi (1991). Here, we consider the prediction of the initial damage surfaces of brittle matrix composites. To this end the micromechanics analysis provides in the absence of thermal and inelastic effects the following relation between the local stress $\boldsymbol{\sigma}^{(\beta\gamma)}$ in the subcell and the externally applied stress $\bar{\boldsymbol{\sigma}}$

$$\boldsymbol{\sigma}^{(\beta\gamma)} = \boldsymbol{B}^{(\beta\gamma)} : \bar{\boldsymbol{\sigma}} \tag{42}$$

where $\boldsymbol{B}^{(\beta\gamma)}$ is the already micromechanically established forth-order stress concentration tensor. Assume for instance that the initial damage surface in the transverse plane $\bar{\sigma}_{22} - \bar{\sigma}_{33}$ is sought. Here all stresses $\bar{\sigma}_{ij} = 0$ except $\bar{\sigma}_{22}$ and $\bar{\sigma}_{33}$. Let

$$\bar{\sigma}_{22} = R\cos\theta, \quad \bar{\sigma}_{33} = R\sin\theta \tag{43}$$

where R is the radial distance to the initial damage surface at polar angle θ. Substituting Eq. (43) in (32) yields that for a given θ

$$R = \min_{over\ all\ matrix\ subcells} \frac{\kappa}{\sqrt{\langle\epsilon_1\rangle^2 + \langle\epsilon_2\rangle^2 + \langle\epsilon_3\rangle^2}} \tag{44}$$

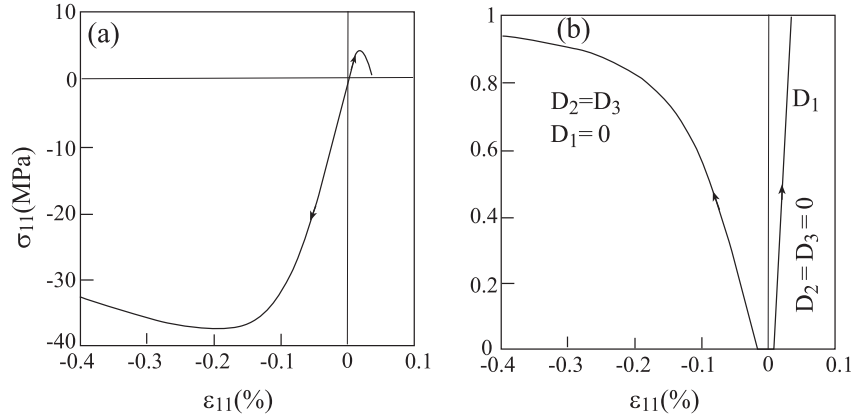

Fig. 9. The response of the unreinforced concrete under tensile and compressive uniaxial stress loading. (a) Stress–strain response, (b) evolution of the anisotropic damage variables with loading.

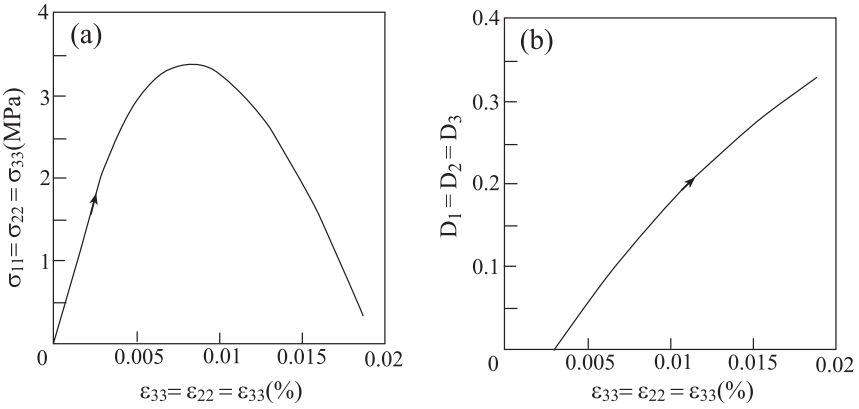

Fig. 10. The response of the unreinforced concrete under tensile hydrostatic loading. (a) Stress–strain response, (b) evolution of the damage variables with loading.

Once this envelope has been generated, any combination of the two values of $\bar{\sigma}_{22}$ and $\bar{\sigma}_{33}$ that initiate the damage can be readily determined.

Next, consider the unidirectional composite that is subjected to an off-axis uniaxial loading. Here the fibers which are oriented in the 1-direction, are rotated around the 3-direction by an angle θ. As a result a new system of coordinates (x,y,z) is obtained such that $z = x_3$. The unixial stress loading is applied in the x-direction which is at angle θ with respect to the fiber direction. Referring to this system of coordinates, the composite is loaded by the application of a stress σ_{xx}, with all components of the stress with respect to this system are zero. In particular, $\theta = 0^\circ$ and 90° correspond to longitudinal and transverse uniaxial stress loading, respectively. In the present case of tensile/compressive off-axis loading the following three stress components are not zero: $\bar{\sigma}_{11}$, $\bar{\sigma}_{22}$ and $\bar{\sigma}_{12}$. The initial damage surface can be determined by replacing Eq. (43) with

$$\bar{\sigma}_{11} = \pm R\cos^2\theta, \quad \bar{\sigma}_{22} = \pm R\sin^2\theta, \quad \bar{\sigma}_{12} = \mp R\sin\theta\cos\theta \tag{45}$$

For a given set of angles θ, R can be determined from Eq. (44). Here too, once this envelope has been generated, the values of applied off-axis tensile or compressive uniaxial stress loading $\pm\sigma_{xx}$ that initiate damage can be readily determined.

4. Applications

The offered theory is implemented herein to investigate the effects of isotropic and anisotropic laws on the response of a metal

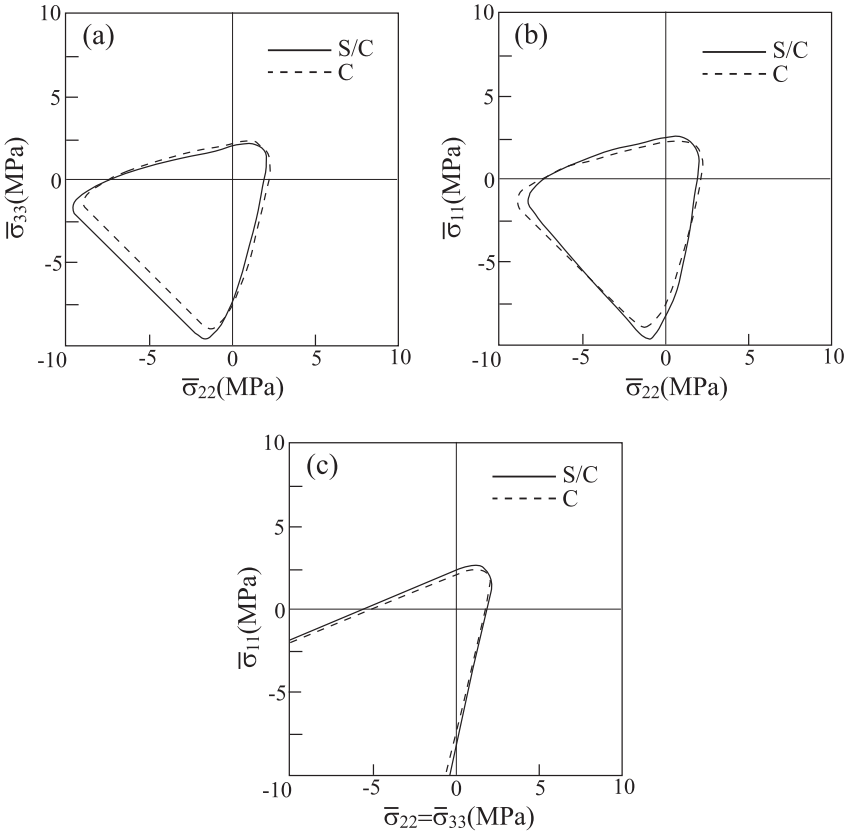

Fig. 11. Initial damage envelopes of the unidirectional steel/concrete (S/C) composite and the unreinforced concrete (C). (a) Initial damage in the transverse $\bar{\sigma}_{33} - \bar{\sigma}_{22}$ plane, (b) Initial damage in the $\bar{\sigma}_{11} - \bar{\sigma}_{22}$ plane, (c) initial damage in the $\bar{\sigma}_{11} - \bar{\sigma}_{22} = \bar{\sigma}_{22}$ plane.

matrix composite. Both the one-way and full thermomechanical coupling micromechanics are employed. Next, the behavior of a concrete reinforced by steel fibers is investigated under various loading conditions. In this latter case initial damage envelopes are generated exhibiting the different behavior of the reinforced concrete under tensile and compressive loadings. The anisotropic damage components D_1, D_2, D_3 and the isotropic damage variable D shown in the following plots pertain to the maximum of the corresponding ones in the ductile or brittle matrix. A typical repeating unit cell of the periodic composite is shown in Fig. 1(d) where the elastic fiber, oriented in the 1-direction, is reinforcing either a ductile or brittle matrix.

4.1. Results for a metal matrix composite with one-way thermomechanical coupling

Consider a unidirectional carbon/metal matrix composite. The elastic carbon fibers are transversely isotropic where the axis of symmetry is oriented in the fibers 1-direction and whose properties are given in Table 1. The properties of the aluminum alloy matrix are given in Table 2 at various temperatures. Unless otherwise mentioned, all results in the following are given with the damage parameters: $S = 0.05$ MPa, $s = 1$ and $\eta = 2.6$, which characterize the aluminum matrix. The fibers volume fraction of this carbon/aluminum system is $v_f = 0.3$.

In Fig. 2, the behavior at room temperature $T = 21\,^{\circ}\mathrm{C}$ of the unreinforced aluminum alloy matrix caused by a uniaxial stress loading in the 1-direction followed by unloading is shown in the following cases. (a) Anisotropic damage is evolving, (b) isotropic damage is evolving, and (c) no damage is taking place $D = 0$. The figure shows the uniaxial stress–strain response $\sigma_{11} - \epsilon_{11}$, the transverse strain response $\epsilon_{22} - \epsilon_{11}$, the evolution of the anisotropic damage variables D_1, $D_2 = D_3 = D_1/2$ and isotropic damage D with applied strain, and the variations of the Young's moduli E_1, $E_2 = E_3$ and E caused by anisotropic and isotropic damage with the applied strain. This figure clearly exhibits the effect of damage on the behavior of the aluminum alloy matrix and whether the damage law is controlled by anisotropic or isotropic law. Although the damage D_1 is very close to D, the damage D_2 in the transverse direction is almost one half of that predicted by the isotopic law. This result affects the transverse Young's modulus E_2 which is seen to be quite different from the E that is developed in the isotropic case.

Fig. 3 shows the response of the unidirectional carbon/aluminum composite to a uniaxial stress loading–unloading applied in the fibers direction at room temperature. It is clearly observed that the axial response $\bar{\sigma}_{11} - \bar{\epsilon}_{11}$ is not affected by the damage law type. The global transverse strain however is sensitive to the adopted damage law. This can be explained by observing the evolution of the anisotropic and isotropic damage variables in the matrix. Although D_1 is quite close to D, $D_2 = D_3$ is significantly different from the latter. Thus, the influence of the type of damage on the transverse response of the composite as exhibited by Fig. 3(b) can be expected.

It should be interesting to study the effect of damage on the spatial stress distribution in the RUC induced by the axial loading. The most interesting internal stress component which is not dominated by fibers is the spatial transverse stress distribution $\sigma_{22} = \sigma_{33}$. In Fig. 4(a)–(c), surface plots of σ_{22} generated at applied global strain of $\bar{\epsilon}_{11} = 0.02$ are shown for anisotropic, isotropic

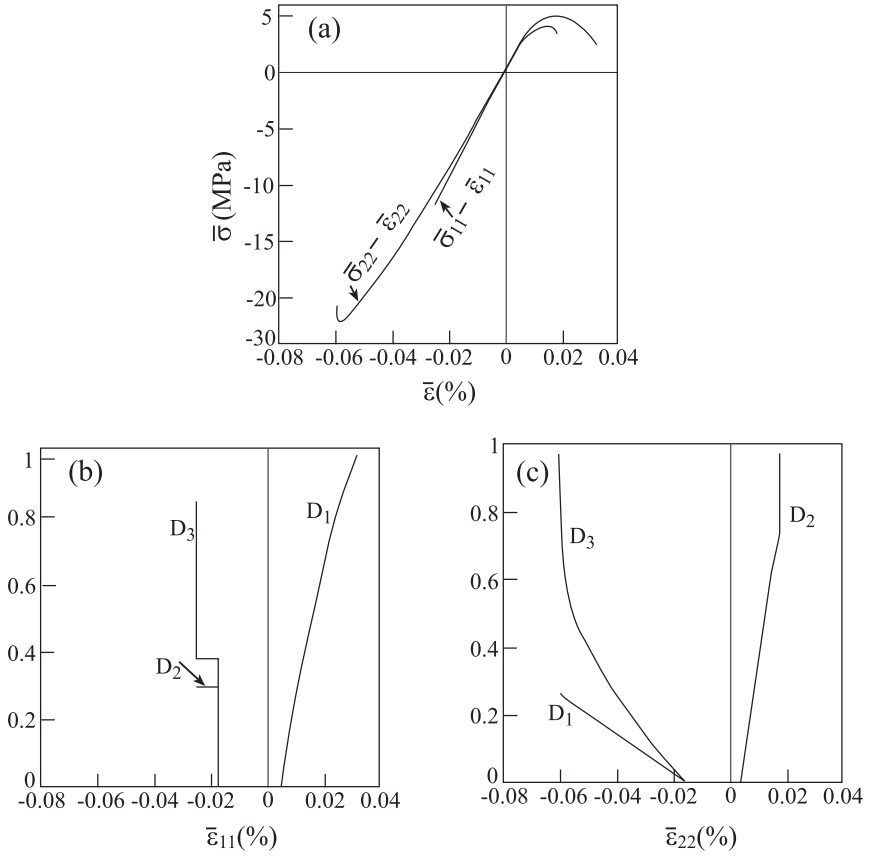

Fig. 12. The response of the steel/concrete under axial and transverse uniaxial stress tensile and compressive loadings. (a) Axial stress–strain $\bar{\sigma}_{11} - \bar{\epsilon}_{11}$ and transverse $\bar{\sigma}_{22} - \bar{\epsilon}_{22}$ responses, (b) evolution of the damage variables in the axial tensile and compressive loadings, (c) evolution of the damage variables in the transverse tensile and compressive loadings.

damage laws as well as $D = 0$, respectively. The effect of damage is clearly noticed by observing the ranges of these induced stresses. For the anisotropic, isotropic damage laws and intact composite ($D = 0$), the values of induced transverse stresses are: $-4.7\ \text{MPa} \leqslant \sigma_{22} \leqslant 6.9\ \text{MPa}$, $-10.6\ \text{MPa} \leqslant \sigma_{22} \leqslant 14.1\ \text{MPa}$ and $-12.1\ \text{MPa} \leqslant \sigma_{22} \leqslant 16.1\ \text{MPa}$, respectively. These variations are significant and clearly show the effect of damage on these internal stresses. It should be noted that in the anisotropic progressive damage law case, the induced transverse stresses are much lower than the isotropic one. The stress concentrations in the former and the latter cases can be seen to be around 4.9 MPa and 11.8 MPa, respectively, which exhibit a significant difference between the anisotropic and isotropic laws. As is expected, the highest values are generated in the intact composite with a stress concentration of about 12.9 MPa.

Contrary to a loading in the axial direction, a loading in the transverse direction (perpendicular to the fibers) leads to a rapid failure. This is shown in Fig. 5 which exhibits the unidirectional composite's response to a uniaxial stress loading in the transverse direction. Fig. 5(a) shows the effect of evolving damage by a comparison with the resulting global response in the absence of damage $D = 0$. The macroscopic composite responses resulting from anisotropic and isotropic damage laws coincide. Fig. 5(b) shows the corresponding evolution of the damage variables in the metallic matrix. In the present transverse loading case, failure of the matrix constituent results from the rapid increase of the D_2, D_3 and D. The axial damage variable D_1 shows a moderate increase which slightly affects the axial global strain.

Fig. 6 exhibits the global $\sigma_{xx} - \epsilon_{xx}$ of the composite that is subjected to off-axis uniaxial stress loading at angle θ to the fibers 1-direction. Comparisons between the responses caused by anisotropic and isotropic damage laws are shown at various off-axis angles. These plots clearly exhibit the influence on the predicted response of the composite and its failure which depends on the chosen progressive damage laws. This effect appears to be significant at the intermediate angles. In Fig. 7, the evolution of the corresponding damage variables are shown. Here too and as

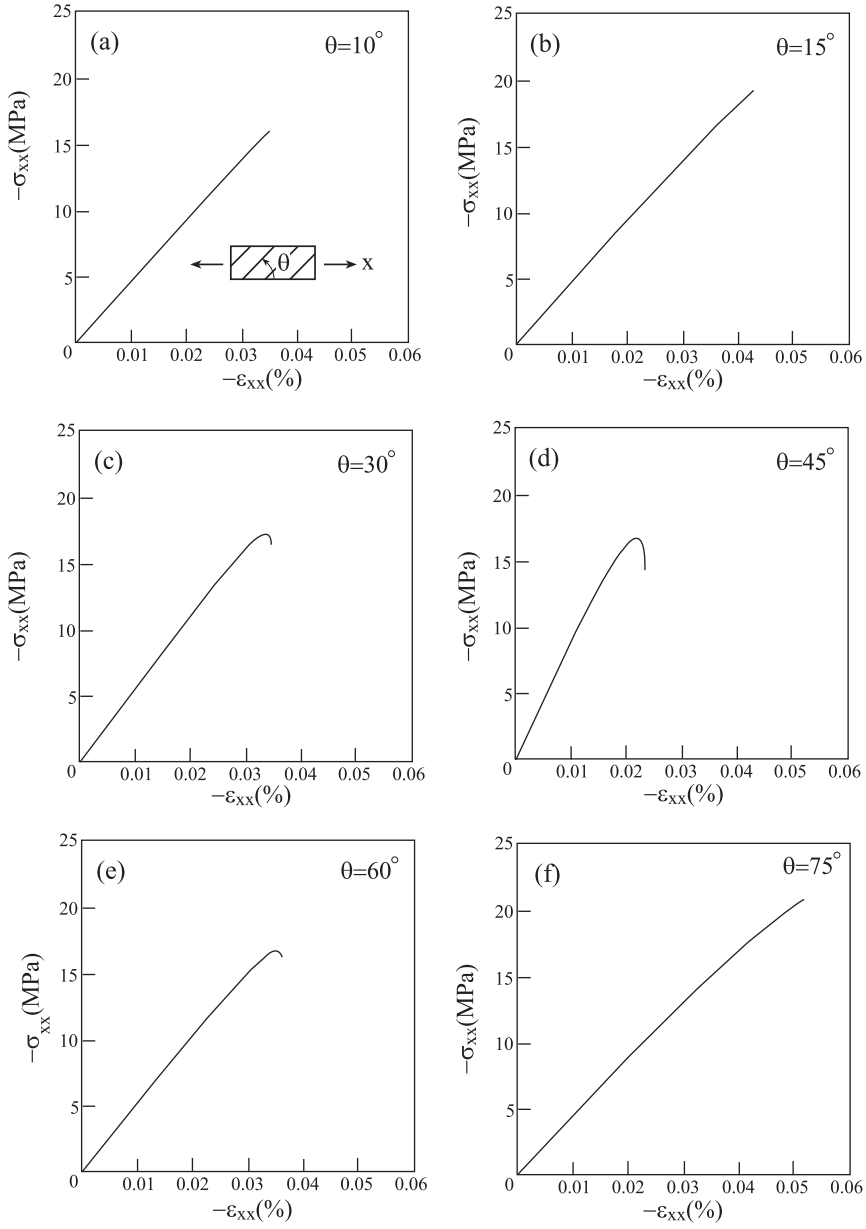

Fig. 13. The global stress-stress responses of the unidirectional steel/concrete composite that is subjected to off-axis compressive uniaxial stress loading at various angles θ with respect to the fibers direction.

expected from the plots of Fig. 6, the damage variables associated with anisotropic and isotropic damage laws significantly differ at the intermediate angles. Similarly, the deterioration of the effective Young's moduli E_1^*, E_2^* and E_3^* of the composite with damage caused by the anisotropic and isotropic damage laws are quite similar for axial and transverse loadings of the composite. For the intermediate off-axis angles however their reductions are different depending on the adopted damage law. For consider for example the off-axis loading at $\theta = 45°$. Initially, $E_1^* = 167$ MPa and $E_2^* = E_3^* = 44.7$ MPa prior to damage initiation. At the final stage of loading just before failure, the anisotropic damage law yields: $E_1^* = 144$ MPa, $E_2^* = 12.5$ MPa and $E_3^* = 38.8$ MPa. The isotropic law yields on the other hand: $E_1^* = 151$ MPa, $E_2^* = 34.4$ MPa and $E_3^* = 31.4$ MPa. It is clearly observed the effect of the damage law is considerable especially for the effective Young's modulus in the 2-direction.

Let us assume that the carbon/aluminum composite is at the cure temperature $T = 371.1$ °C, see Table 2, at which it is microscopically stress-free. The composite is cooled from this initial state while it is kept macroscopically stress-free, i.e., $\bar{\boldsymbol{\sigma}} = 0$. In Fig. 8(a) and (b), the global axial $\bar{\epsilon}_{11}$ and transverse $\bar{\epsilon}_{22} = \bar{\epsilon}_{33}$ strains are shown during a cycle of cooling and re-heating while adopting the anisotropic and isotropic damage laws in the metallic matrix. It is clear that yielding and plastic flow take place during the cooling process which also cause the initiation and propagation of damage. Thus far the damage parameter S at room temperature has been chosen to have the value of 0.05 MPa. At elevated temperature the value of S must be lower (for steel for example, Lemaitre and Desmorat (2005) suggested that the value of S at $T = 580$ °C is about 35 times lower than its corresponding value at room temperature). To this end and for illustration, the value of $S = 0.005$ MPa has been chosen which is just ten times lower.

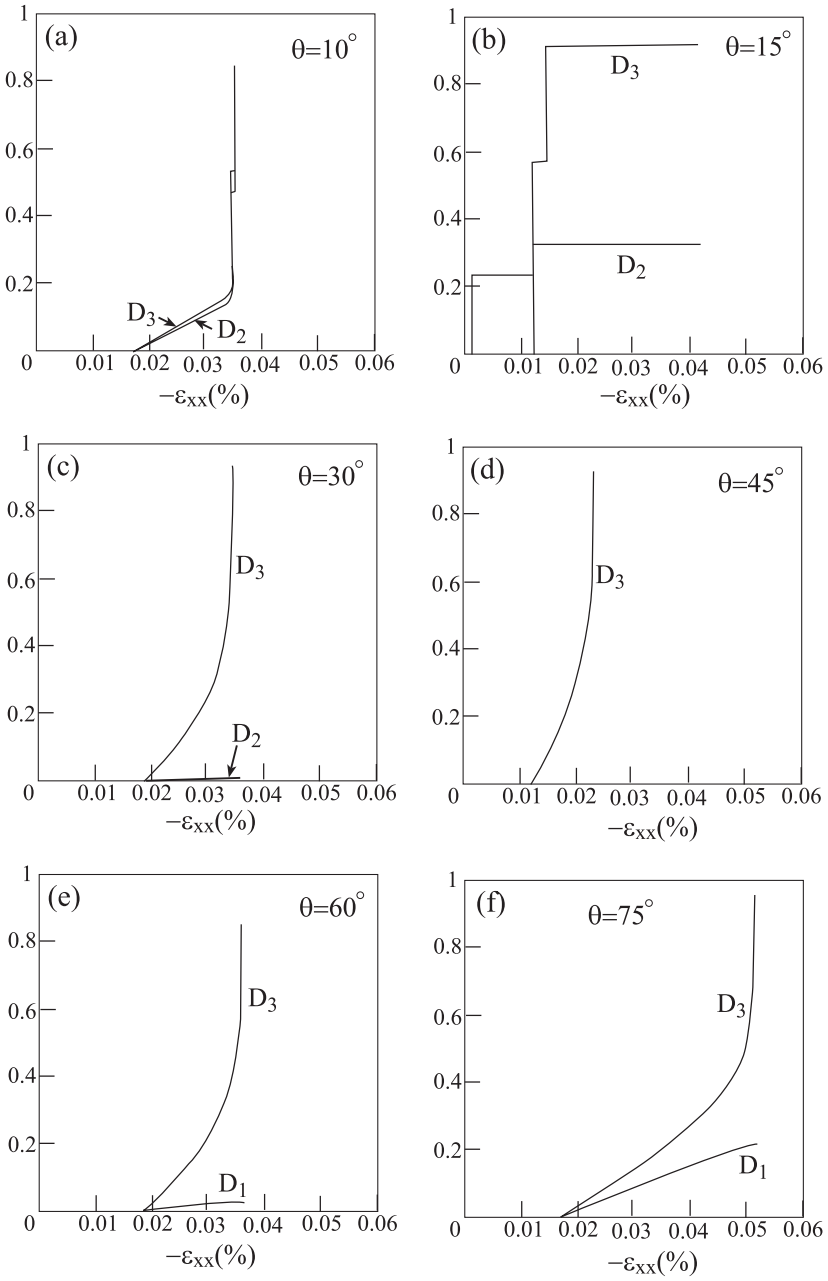

Fig. 14. The evolution of the damage variables in the metallic matrix caused by the off-axis compressive loading of the unidirectional carbon/aluminum composite.

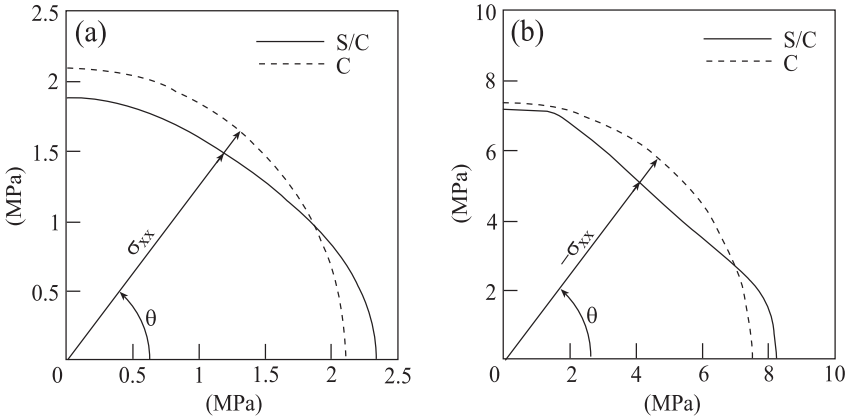

Fig. 15. Variation of the values of the off-axis uniaxial stress loading σ_{xx} which initiate damage with the off-axis angle θ of the steel/concrete (S/C) and unreinforced concrete (C). (a) Tensile off-axis loading, (b) compressive off-axis loading.

Table 4
Elastic and thermal parameters of the isotropic Al_2O_3 fibers.

E (GPa)	v	α (10^{-6}/K)	k (W/(mK))	ρc_v (MJ/(m^{3}K))
400	0.24	16.3	30	3.1

E, v, α, k and ρc_v denote the Young's modulus, Poisson's ratio, coefficient of thermal expansion, thermal conduction and heat capacity, respectively.

Fig. 8 shows that for the value of $S = 0.05$ MPa, the anisotropic and isotropic laws predict identical response during cooling and re-heating. For the lower value of $S = 0.005$ MPa however, the responses according to two laws are different. The macroscopic transverse strains on the other hand are insensitive to the adopted damage type. In Fig. 8(c)–(e), the evolution of the damage variables are shown. A comparison between the anisotropic and isotropic damage variables shows that the damage variable in the isotropic case evolves to a higher value than the corresponding anisotropic one. This explains the reason for the different behavior in the low value of parameter S exhibited by the plots of Fig. 8(a). The macroscopic axial and transverse strains that are developed during cooling from the cure to room temperature give rise to residual stresses. According to the graphs of in Fig. 8(a), these residual stresses depend on the damage parameters and whether they are controlled by anisotropic or isotropic laws. This implies that a subsequent mechanical tensile/compressive loading of the composite at room temperature should be appreciably affected by the type of damage evolution.

4.2. Results for a concrete matrix composite

Presently, we consider a unidirectional steel/concrete composite. The elastic steel fibers are isotropic that are characterized by a Young's modulus of $E = 200$ GPa and Poisson's ration $v = 0.32$. The constitutive equations of the concrete matrix are determined from the Gibbs function (29) in conjunction with the damage evolution law given by Eq. (35). The Young's modulus and Poisson's ration ratio of the concrete together with the non-dimensional parameters a, a' and κ_0 are given in Table 3. The fibers volume ratio is chosen as $v_f = 0.03$.

In Fig. 9(a), the behavior of the unreinforced concrete subjected to tensile and compressive uniaxial stress loadings is shown. This plot coincides with the stress–strain curve of Lemaitre and Desmorat (2005). The different response to tensile and compressive loading which is characteristic for the concrete is well exhibited. The evolutions of the damage variables that are controlled by the anisotropic damage law are shown in Fig. 9(b). For the tensile loading, $D_1 \neq 0$ and $D_2 = D_3 = 0$. The damage variable D_1 rises sharply from 0 to 1 with the applied tensile strain where complete failure is obtained. For the compressive loading, on the other hand, $D_1 = 0$ and $D_2 = D_3 \neq 0$. These damage variables control the response in this region and are seen to rise moderately with the applied loading. It is also interesting to observe the response of the unreinforced concrete to a hydrostatic loading. In accordance with the constitutive equations of the concrete, damage does not evolve under pressure (compressive loading). Therefore, Fig. 10 shows the response under positive hydrostatic loading $\epsilon_{11} = \epsilon_{22} = \epsilon_{33} > 0$ together with the damage variables evolutions all of which are equal. Failure of the material can be expected before a loading of $\epsilon_{11} = 0.02$ where the damage variables increase abruptly to 1.

The initial damage envelopes of the monolithic concrete and the steel/concrete composite are shown in Fig. 11. In this figure, the envelopes are shown in the $\bar{\sigma}_{33} - \bar{\sigma}_{22}$, $\bar{\sigma}_{11} - \bar{\sigma}_{22}$ and $\bar{\sigma}_{11} - \bar{\sigma}_{22} = \bar{\sigma}_{33}$ planes. Both Fig. 11(a) and (b) clearly show the effect of tensile and compressive loading on the damage initiation. Fig. 11(c) exhibits the effect of tensile and compressive hydrostatic loadings on damage initiation, and its absence in the latter case. The closeness of the initial damage envelopes of the composite and the unreinforced concrete is due to the fact that the volume ratio of the steel is very low which is characteristic to steel/concrete composites.

The response of the steel/concrete unidirectional composite to uniaxial stress tensile and compressive loadings applied in the axial (parallel to the fibers) and transverse (perpendicular to the fibers) are shown in Fig. 12(a). The locations of failure in both cases can be clearly observed. The corresponding evolution of the anisotropic damage variables to these two types of loadings are shown in Fig. 12(b) and (c). These two figures show that failures under axial tensile and compressive loadings are dominated by the

Table 5
Elastic, plastic and thermal parameters of an isotropic elastoplastic aluminum matrix.

E (GPa)	v	α (10^{-6}/K)	Y_0 (MPa)	H_0 (GPa)	k (W/(mK))	ρc_v (MJ/(m^{3}K))
72.4	0.33	22.5	371.5	23	116.7	2.25

E, v, α, σ_y, H_0, k and $\rho\ c_v$ denote the Young's modulus, Poisson's ratio, coefficient of thermal expansion, yield stress, linear hardening coefficient, thermal conduction and heat capacity, respectively.

evolution of D_1 and D_3, respectively. The variable D_2 increases moderately under compression in this case while $D_1 = 0$. Under transverse tensile and compressive loadings on the other hand, failures are attributed to the increase of the anisotropic damage variables D_2 and D_3, respectively. Consequently, the effect of anisotropic damage model appears to be significant in the present case.

Let us consider the steel/concrete unidirectional composite when it is subjected to off-axis compressive uniaxial stress loadings. The resulting responses up to failure are shown in Fig. 13 for various off-axis angles θ. The corresponding evolution damage of the damage variables are shown in Fig. 14. Tracking these variables at the various off-axis angles shows that $D_1 = 0$ in the low off-axis angles with D_2 decreasing and then vanishing at $\theta \geqslant 45$. For $\theta > 45°$, the damage variable D_1 increases from zero with the increase of θ. It is interesting to observe that D_3 appears to be dominant in all off-axis angles The values of uniaxial stress loading σ_{xx} at which damage initiates in the concrete matrix of the steel/concrete composite and in the unreinforced matrix at a given off-axis angle θ are shown in Fig. 15. Both applied tensile and compressive σ_{xx} are shown in this figure, and the differences between damage initiation in both cases are clearly displayed.

4.3. Results for a metal matrix composite with full thermomechanical coupling

Extensive investigation of the effects of full thermomechanical coupling in metal matrix composites have been presented by Aboudi (2008). It turned out that the most interesting and important result of this micromechanical analysis was the temperature field induced by an applied mechanical loading (which would be absent in the case of one-way thermomechanical coupling). Under cyclic mechanical loading this temperature field may significantly grow and affects the subsequent composite's behavior. For shape memory reinforced composites for example, the induced temperature field affects the shape memory alloy itself by changing its properties (Aboudi and Freed, 2010). Presently, let us adopt the same Al_2O_3/aluminum unidirectional composite which was employed in Aboudi (2008) and for which extensive results were shown.

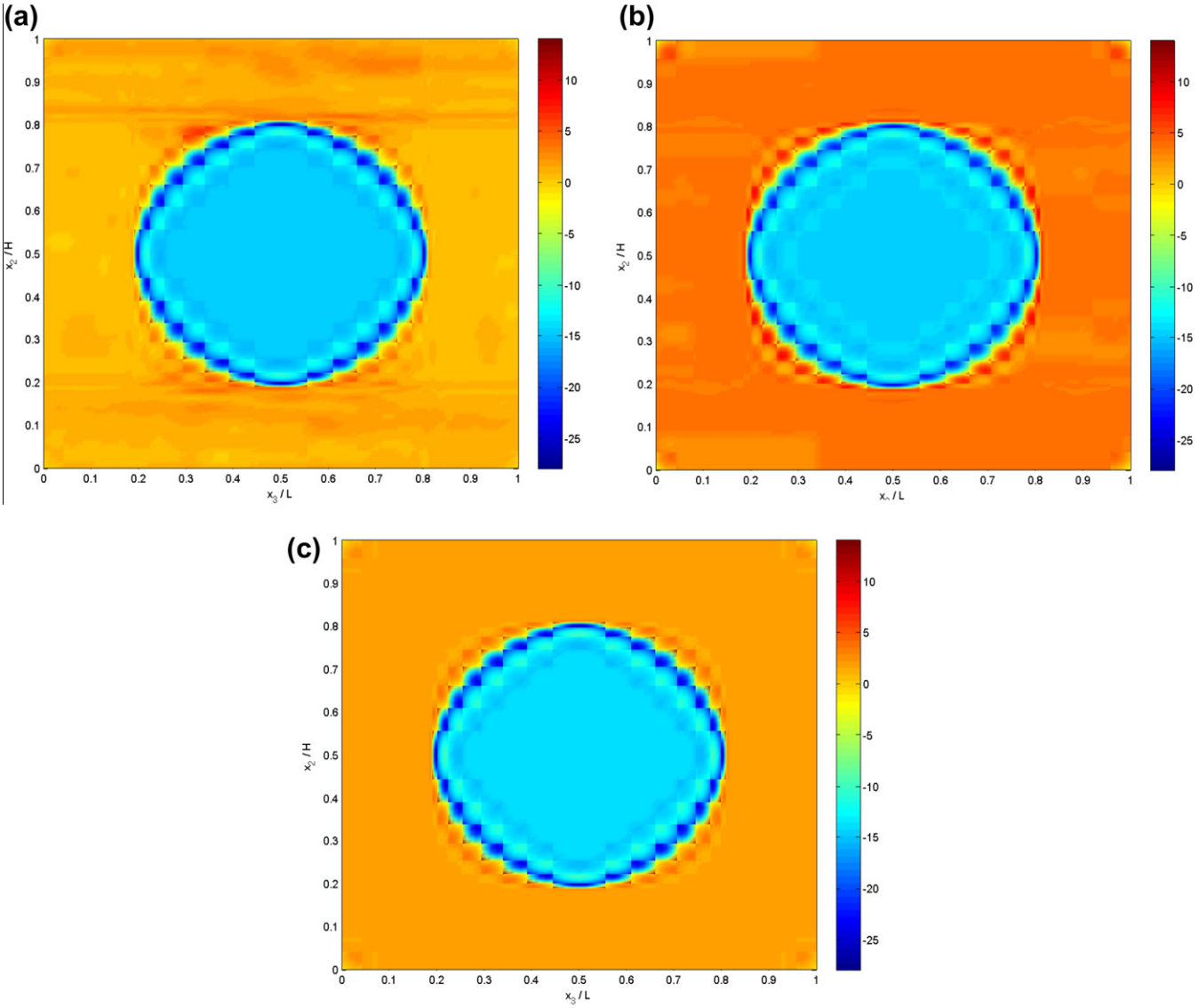

Fig. 16. Surface plots of the internal spatial distributions of the temperature deviations $\Delta T(K)$ in the RUC, generated by applying a longitudinal uniaxial stress loading of the unidirectional Al_2O_3/aluminum composite at $\bar{\epsilon}_{11} = 0.0258$ (just before the ultimate failure of the composite with anisotropic damage law). (a) ΔT distribution generated by employing the anisotropic damage law in the matrix, (b) ΔT distribution generated by employing the isotropic damage law in the matrix, (c) ΔT distribution generated in the intact composite.

The thermomechanical properties of the elastic Al_2O_3 fibers and the aluminum matrix are given by Tables 4 and 5, respectively, and fiber volume fraction is $v_f = 0.3$.

Let the Al_2O_3/aluminum composite be subjected to a longitudinal uniaxial stress loading in the fiber direction. This mechanical loading is continued up to failure of the composite, controlled by anisotropic damage law in its matrix, at $\bar{\epsilon}_{11} = 2.58\%$. The composite with isotropic damage law, on the other hand, fails at a somewhat higher strain: $\bar{\epsilon}_{11} = 2.8\%$. Fig. 16(a)–(c) exhibit the resulting induced spatial temperature deviation distributions in the RUC caused by the full thermomechanical coupling, for the cases of anisotropic damage law, isotropic damage law and the case with zero damage ($D = 0$) in the matrix, respectively, at $\bar{\epsilon}_{11} = 2.58\%$. It can be observed that the temperature distribution in the composite with anisotropic damage is quite different from the distribution obtained in the isotropic damage case. The undamaged composite exhibits, on the other hand, a temperature distribution which somewhat similar to the anisotropic case. Although the ranges of the temperature deviations obtained from the anisotropic and isotropic damage laws appear to be close, the anisotropic law is seen to exhibit a lower induced temperature distribution. This can be also observed by examining Fig. 17 in which the development of the averages of the induced spatial temperature deviations $\Delta\overline{T}$ with the applied loading are shown in the above three cases of anisotropic, isotropic damage laws in the matrix and the intact composite ($D = 0$). It can be observed that after initial yielding, the average temperature in the composite with anisotropic damage law deviates from the isotropic and zero damage cases, exhibiting the lower values. Hence, it can be concluded that the induced temperature in the anisotropic case exhibits lower values than the isotropic and undamaged cases. Consequently, it is probably possible to employ this information about the induced spatial temperature to estimate the amount of damage that takes place in the metallic matrix of the composite, especially when the composite is subjected to a cyclic loading which generates much higher induced temperatures. Finally, it should be mentioned that for the considered metal matrix composite system, the rate of plastic work of the inelastic matrix is a major contribution to the heat release as compared to the heat caused by the damage process. The latter contribution being positive, causes an increase in the induced temperature deviation. For example, the contributions of this term to the induced temperature deviation spans in the composite with anisotropic and isotropic damage laws at $\bar{\epsilon}_{11} = 2.58\%$ are: 6 K and 9.4 K, respectively, which form temperature increase of 17% and 30%.

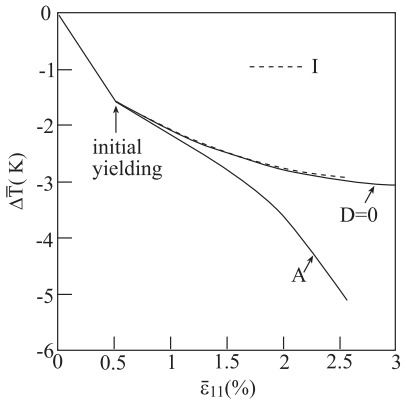

Fig. 17. Average of the temperature deviations $\Delta\overline{T}(K)$ induced in the unidirectional Al_2O_3/aluminum composite by applying a longitudinal uniaxial stress up to failure. (A) and (I) denote the cases with anisotropic and isotropic evolution laws, respectively, and $D = 0$ corresponds to the intact composite.

5. Conclusions

The aim of the present investigation was to simulate and assess the effects of anisotropic damage evolution in ductile and brittle matrix unidirectional composites. These effects can be detected either by comparison with the isotropic damage evolution results or by tracking the disparity of the evolutions of the principal damage variables (i.e., D_1, D_2 and D_3). The anisotropic damage law affects differently the various elements of the effective compliance tensor of the composite and thus represents the overall behavior of the composite as an orthotropic material. For example, the effective Young's modulus E_1^* in the fibers direction is affected differently from the effective Young's modulus E_2^* in the transverse direction. The same applies to thermal conductivities in the various directions. In contrast, isotropic damage law affects these moduli in the same manner. In the metal matrix composite, a far lower values of stress concentrations and induced spatial temperature distributions are exhibited by the results obtained from the anisotropic damage law. In addition, for applied off-axis loadings, the anisotropic damage law predicts failure of the composite at an earlier stage than the isotropic law. When the metal matrix composite is cooled down from its processing elevated temperature, the anisotropic damage affects the induced residual stresses components differently. This fact influences the subsequent mechanical loading of the composite at room temperature. Initial damage envelopes in metal matrix composites coincide with the initial yield surfaces. For the specific brittle matrix composite that has been considered, initial damage surfaces have been generated under various types of loading. For off-axis compressive loading, the earliest failure of the composite was obtained at angle $\theta = 45^\circ$ to the fibers where only one component of the damage is predominantly active. The present results show that anisotropic damage formulation is necessary in analyzing the behavior of damage progression in composites. This is because the damage mechanism is controlled by the spatial distribution of the local fields in the composite. These local effects have been shown to be sensitive to the anisotropic damage evolution.

The present investigation has been based on the anisotropic damage laws of Lemaitre and Desmorat (2005). Adopting other anisotropic damage laws are possible (e.g. Voyiadjis and Park, 1996) thus enabling, by their coupling with HFGMC, the modeling of evolving damage in metal, polymeric and ceramic matrix composites. In the present investigation the effect of crack closure, as a result of which different responses in tension and compression are exhibited, have been neglected. The present approach can be extended to incorporate these effects in the ductile and brittle matrices. In addition, damage thresholds prior to which degradations do not start, and critical damage values beyond which the material in the subcell fails and should be removed, can be included in the offered analysis.

The present investigation considered unidirectional composites. Extensions to laminated materials can be performed. In addition, the present micromechanical theory with progressive damage can be coupled to a finite element software to investigate the behavior of composite structures with propagating damage in the phases, thus forming a multiscale micro–macro-structural analysis.

Acknowledgment

The author is grateful to Dr. Steven M. Arnold, NASA Glenn Research Center, for his suggestion to investigate the effect of damage in the presence of full thermomechanical coupling.

References

Aboudi, J., 1991. Mechanics of Composite Materials: A Unified Micromechanical Approach. Elsevier, Amsterdam.

Aboudi, J., 2004. The generalized method of cells and high-fidelity generalized method of cells micromechanical models-a review. Mech. Adv. Mater. Struct. 11, 329–366.
Aboudi, J., 2008. Thermomechanically coupled micromechanical analysis of multiphase composites. J. Eng. Math. 61, 111–132.
Aboudi, J., Freed, Y., 2010. Micromechanical modeling of shape memory alloy composites. In: Chen, H.R. (Ed.), Shape Memory Alloys: Manufacture, Properties and Applications. Nova Science Publishers, New York, pp. 371–423.
Barbero, E.J., 2008. Finite Element Analysis of Composite Materials. CRC Press, Boca Raton, Florida.
Bednarcyk, B.A., Aboudi, J., Arnold, S.M., 2010. Micromechanics modeling of composites subjected to multiaxial progressive damage in the constituents. AIAA J. 48, 1367–1378.
de Souza Neto, E.A., Perıíl, D., Owen, D.R.J., 2008. Computational Methods For Plasticity. Wiley, Chichester, UK.
Haj-Ali, R.M., 2009. Cohesive micromechanics: A new approach for progressive damage modeling in laminated composites. Int. J. Damage Mech. 18, 691–719.
Haj-Ali, R., Aboudi, J., 2009. Nonlinear micromechanical formulation of the high fidelity generalized method of cells. Int. J. Solids Struct. 46, 2577–2592.
Haj-Ali, R., Aboudi, J., 2010. Formulation of the high-fidelity generalized method of cells with arbitrary cell geometry for refined micromechanics and damage in composites. Int. J. Solids Struct. 47, 3447–3461.
Kachanov, L., 1986. Introduction to Continuum Damage Mechanics. Springer.
Krajcinovic, D., 1996. Damage Mechanics, North-Holland Series in Applied Mathematics and Mechanics, North Holland.
Lemaitre, J., 1985a. A continuous damage mechanics model for ductile fracture. J. Eng. Mater. Tech. 1985a (107), 83–89.
Lemaitre, J., 1985b. Coupled elasto-plasticity and damage constitutive equations. Comput. Meth. Appl. Mech. Eng. 51, 31–49.
Lemaitre, J., 1996. A Course on Damage Mechanics. Springer, New York.
Lemaitre, J., Chaboche, J.L., 1990. Mechanics of Solid Materials. Cambridge University Press, Cambridge.
Lemaitre, J., Desmorat, R., 2005. Engineering Damage Mechanics. Springer, Berlin.
Lemaitre, J., Desmorat, R., Sauzay, M., 2000. Anisotropic damage law of evolution. Eur. J. Mech. A Solids (19), 187–208.
Skrzypek, J., Ganczarski, A., 1999. Modeling of Material Damage and Failure of Structures: Theory and Applications, Springer.
Talreja, R., 1985a. A continuum mechanics characterization of damage in composite materials. Proc. R. Soc. A, 399, 195–216.
Talreja, R., 1985b. Transverse cracking and stiffness reduction in composite laminates. J. Compos. Mater. 19, 355–375.
Talreja, R., 1994. Damage Mechanics of Composite Materials. Elsevier Science. vol. 9.
Voyiadjis, G.Z., Deliktas, B., 1997. Damage in MMCs using the GCM: Theoretical formulation. Composites B 28B, 597–611.
Voyiadjis, G.Z., Kattan, P.I., 1999. Advances in Damage Mechanics: Metal and Metal Matrix Composites. Elsevier, Amsterdam.
Voyiadjis, G.Z., Kattan, P.I., 2005. Damage Mechanics. Taylor & Francis, Boca Raton, Florida.
Voyiadjis, G.Z., Park, T., 1996. Anisotropic damage for the characterization of the onset of macro-crack initiation in metals. J. Damage Mech. 5, 68–92.
Wu, J.Y., Li, J., Faria, R., 2006. An energy release rate-based plastic-damage model for concrete. Int. J. Solids Struct. 43, 583–612.